2. emissions near 200° CML are from a northern-hemisphere source and are LH polarized when viewed from above the sunlit hemisphere but are RH polarized when viewed from above Jupiter's nightside;
3. there exists a complementary southern hemisphere source near CML ~20° for an observer at southern jovigraphic latitudes;
4. a model of the northern-hemisphere source that emits in the left-hand-ordinary mode from a region above Jupiter's dayside ionosphere in the northern hemisphere is consistent with all the observations; and
5. refraction of bKOM waves as they propagate through or over the Io plasma torus is likely to influence the spectral properties observed for bKOM.

For bKOM, we do not yet know:

1. how far above 1 MHz the emission can extend;
2. what is the origin of the drifting patterns seen in dynamic spectra;
3. what is the origin of the observed temporal variations in bandwidth and intensity; and most importantly,
4. what is the emission mechanism.

For nKOM, we know:

1. the emission occurs only over a narrow band of frequencies comparable to the electron plasma frequency near the edge of the Io plasma torus;
2. the repetition rate of the emission is slower than the System III rate by an amount comparable to the corotation lag in the outer edge of the Io plasma torus; and
3. the emission is intermittent, being active for days at a time then disappearing for several days and then reappearing without apparently changing its location in the "not-quite-corotating" frame.

For nKOM, we do not yet know:

1. what causes the polarization reversals often seen during an event;
2. what causes the episodic appearance and disappearance of the emission; and fundamentally,
3. what is the emission mechanism.

ACKNOWLEDGMENTS

The authors are grateful to their colleagues, T. J. Birmingham, M. L. Goldstein, S. Gulkis, M. L. Kaiser, and W. S. Kurth, for their very thorough review and constructive comments on earlier versions of this chapter. We thank J. J. Schauble and J. R. Thieman for providing unpublished data for Figures 7.1 and 7.15, respectively. We also thank B. C. Holland, F. H. Hunsaker, and L. A. White for their untiring efforts in producing the original typescript and most of the illustrations. We acknowledge the partial support of NASA through grant NAGW-196.

8

PLASMA WAVES IN THE JOVIAN MAGNETOSPHERE

D. A. Gurnett and F. L. Scarf

The recent Voyager encounters with Jupiter have now provided us with the first comprehensive investigation of plasma waves in the magnetosphere of Jupiter. The most striking feature of the Jovian plasma wave observations is the close similarity to the plasma-wave phenomena observed in the Earth's magnetosphere. Essentially, all major types of plasma waves detected in the Jovian magnetosphere have analogs in the Earth's magnetosphere. These include, for example, electrostatic waves near and upstream of the bow shock, electromagnetic continuum radiation, lightning- generated whistlers, whistler-mode chorus and hiss, electrostatic electron cyclotron and upper hybrid emissions, and broadband electrostatic noise.

8.1. Introduction

Any waves that are influenced by the presence of a plasma are called plasma waves. Because wave-particle interactions in a collisionless plasma produce scattering and thermalization effects somewhat similar to collisions in an ordinary gas, plasma waves are now recognized as being of fundamental importance for understanding the equilibrium state of planetary magnetospheres. In the Earth's magnetosphere, wave-particle interactions are known to be responsible for heating the solar wind at the bow shock, for the diffusion that allows plasma to enter the magnetosphere, and for the pitch-angle scattering that causes the loss of energetic particles trapped in the magnetic field. A large number of different types of waves can occur in planetary magnetospheres. The properties of some of the more important plasma wave modes are summarized in Table 8.1. In general, plasma waves can be classified as either electromagnetic, which have both electric and magnetic fields, or electrostatic, which have no magnetic field. The electromagnetic modes include two free space modes that can escape from the plasma and be detected remotely and several internal modes, such as the whistler mode, that cannot escape from the plasma. Typically, the electromagnetic modes tend to have propagation velocities near the speed of light. The electrostatic modes, on the other hand, tend to have much lower propagation velocities with properties somewhat similar to sound waves in an ordinary gas. At low frequencies, below the ion cyclotron frequency, plasma waves display a fluidlike behavior involving the bulk motion of the entire plasma. Two such modes, called the shear and compressional Alfvén waves, are the principal mechanisms by which all fluid disturbances are propagated through a plasma. For a further review of the types of wave modes that can exist in a plasma, the reader is referred to one of the standard texts on the subject, for example, Stix [1962] or Krall and Trivelpiece [1973].

The recent Voyager encounters with Jupiter now provide us with the first comprehensive investigation of plasma waves in the magnetosphere of Jupiter. The most striking feature of the Jovian plasma-wave observations is the very close similarity to the plasma-wave phenomena observed in the Earth's magnetosphere. Essentially, all of the major types of plasma waves detected in the Jovian magnetosphere have analogs in the Earth's magnetosphere. These include, for example, electrostatic waves near and upstream of the bow shock, electromagnetic continuum radiation, lightning-generated

Table 8.1. *Plasma wave modes*

Plasma wave mode	Frequency range	Electromagnetic/ electrostatic	Free energy source
Langmuir mode (electron plasma oscillation)	$\omega \simeq \omega_{pe}$	Electrostatic	Beam ($\partial f/\partial v_{\parallel} > 0$)
Ion-acoustic mode	$\omega \lesssim \omega_{pi}$	Electrostatic	Drift between electrons and ions
Electron Bernstein modes (electron cyclotron waves)	Bands near $\omega \simeq (n + 1/2)\omega_{ce}$	Electrostatic	Ring distribution (electrons) ($\partial f_e/\partial v_{\perp} > 0$)
Ion Bernstein modes (ion cyclotron waves)	Bands near $\omega \simeq (n + 1/2)\omega_{ci}$	Electrostatic	Ring distribution (ions), field-aligned currents
Free space (R,X) mode	$\omega > \omega_{R=0}$	Electromagnetic	Beam, loss cone
Free space (L,O) mode	$\omega > \omega_{pe}$	Electromagnetic	Beam, loss cone, coupling to electrostatic waves
Z-mode	$\omega_{UHR} > \omega > \omega_{L=0}$	Electromagnetic, electrostatic near ω_{UHR}	Beam ($\partial f/\partial v_{\parallel} > 0$)
Whistler mode	$\omega < \text{Min}\ \{\omega_{ce}, \omega_{pe}\}$	Electromagnetic, electrostatic near ω_{LHR}	Loss cone, beam above ω_{LHR}.
Alfvén modes (shear and compressional)	$\omega << \omega_{ci}$	Electromagnetic	Pressure anisotropies

Note: $\omega_{R=0} = \omega_{ce}/2 + \sqrt{(\omega_{ce}/2)^2 + \omega_{pe}^2}$ $\qquad \omega_{UHR} = \sqrt{\omega_{ce}^2 + \omega_{pe}^2}$

$\omega_{L=0} = -\omega_{ce}/2 + \sqrt{(\omega_{ce}/2)^2 + \omega_{pe}^2}$ $\qquad \omega_{LHR} \simeq \sqrt{\omega_{ce}\,\omega_{ci}}$, if $\omega_{pe} >> \omega_{ce}$

whistlers, whistler-mode chorus and hiss, electrostatic electron cyclotron and upper hybrid emissions, and broadband electrostatic noise. Because all of these plasma-wave phenomena have received extensive study in the Earth's magnetosphere over the past few years, it has been possible to make rapid progress in the initial identification and first-order understanding of nearly all of the plasma waves observed in the Jovian magnetosphere. In this section, we review the Jovian plasma-wave observations and discuss the relationships and similarities to plasma-wave observations in the terrestrial magnetosphere.

The first indication of important nonthermal wave emission processes at Jupiter was obtained by Burke and Franklin [1955], who discovered that Jupiter was a strong radio emitter in the decameter wavelength range. A few years later, the detection of synchrotron radiation at much shorter wavelengths, in the microwave region of the spectrum, demonstrated that Jupiter had a radiation belt with a substantial population of trapped electrons. Even though no in situ plasma-wave measurements were available prior to the Voyager observations, strong indirect evidence was available that other local plasma-wave emissions existed that could not be detected remotely from the planet. In developing models of the Jovian radiation belts before the Pioneer encounters with Jupiter, several investigators [Kennel, 1972; Thorne and Coroniti, 1972; Coroniti, 1974] considered the effect of unstable whistler-mode and ion-cyclotron waves on the equilibrium energetic particle distributions in the Jovian magnetosphere. The wave generation processes were expected to be similar to the terrestrial radiation belts, where the loss cone imposed by the atmosphere assures that the whistler mode and ion-cyclotron mode will be unstable if the trapped particle fluxes are sufficiently high. According to the limiting flux theory of Kennel and Petschek [1966] pitch-angle scattering by whistler and ion-cyclotron waves produces an upper limit to the trapped particle intensities that can occur in a radiation belt.

The case for the existence of whistler-mode emissions in the inner magnetosphere of Jupiter was strengthened considerably by the Pioneer 10 and 11 energetic electron measurements, which showed the occurrence of hat-shaped pitch-angle distributions with maximum intensities perpendicular to the magnetic field [Van Allen et al., 1975; Fillius et al., 1976]. Pitch-angle distributions of this type are observed in the terrestrial magnetosphere and are generally believed to arise from pitch-angle scattering by whistler-mode waves [Lyons, Thorne, and Kennel, 1971, 1972]. Further detailed analyses of the Pioneer data by several investigators, including Scarf and Sanders [1976], Coroniti [1975], Baker and Goertz [1976], Barbosa and Coroniti [1976], and Sentman and Goertz [1978], provided specific estimates of the frequency range and intensity of the whistler-mode emissions. These studies suggested, for example, that whistler-mode magnetic field intensities of a few milligammas could be expected in the frequency range of a few kilohertz. Predictions of other types of plasma waves were less specific and were based more on analogies with the Earth's magnetosphere. Scarf [1976] suggested, for example, that electrostatic waves driven by electrons and ions streaming into the solar wind should be observed upstream of the bow shock and that current-driven instabilities should be observed in the field-aligned current system produced by the Io interaction. In our original proposal for the Voyager plasma-wave investigation we also suggested that the local electron concentration could be determined from the cutoff of trapped continuum radiation at the local electron plasma frequency, similar to the continuum radiation cutoff observed in the Earth's magnetosphere [Gurnett and Shaw, 1973]. As it turns out, continuum radiation was detected at Jupiter and the plasma-frequency cutoff has proven to be a valuable method of providing absolute, sheath-independent measurements of the electron concentration in the Jovian magnetosphere.

A complete discussion of the Voyager plasma wave observations involves results that depend somewhat on the instrument characteristics; therefore, a brief review of the instrumentation is useful. For a complete description of the Voyager plasma wave instrument, see Scarf and Gurnett [1977]. Because the plasma-wave investigation was added to the Voyager mission relatively late in the development phase of the project, the available mass, power, and telemetry allocations were minimal. Consequently, even though it was desirable to measure both the electric and magnetic fields of plasma waves, only electric field measurements were possible. Electric-field measurements are obtained using two orthogonal 10 m antennas that are shared with the planetary radio-astronomy experiment [see Warwick et al., 1977]. Voltages from the 10 m elements are combined differentially to form an electric dipole antenna with an effective length of about 7 m. Two methods are used to process the signals from the electric antenna. First, for survey analyses, a 16-channel spectrum analyzer is used to make absolute electric-field spectral-density measurements at 16 logarithmically spaced frequencies from 10 Hz to 56 kHz. Typically, this spectrum analyzer provides one complete frequency scan every 4 s with a dynamic range of 100 db. Second, for detailed high-resolution spectrum analyses, the electric-field waveform in the frequency range from about 50 Hz to 14 kHz is transmitted to the ground using the high rate (115 kbs) imaging telemetry system. Because the wideband measurement must be time shared with the imaging system, wideband high-resolution spectrum measurements are only available for short intervals, usually consisting of isolated 48-s bursts. Because the wideband data transmission employs an automatic gain control receiver to maintain the signal within the dynamic range of the telemetry system, no absolute field-strength measurements can be obtained from the wideband data alone. The wideband waveform measurements do, however, provide a valuable capability for analyzing complex plasma-wave phenomena, because the broadband measurements give essentially continuous coverage in frequency and time, subject only to the constraints imposed by $\Delta f \, \Delta t \sim 1$.

In describing the plasma-wave results obtained by Voyager we will discuss the observed phenomena in several broad categories, ordered more or less according to the radial distance at which each phenomenon was first observed. In general, the results presented are limited to discussions of plasma waves confined to the near vicinity of the planet. For a discussion of freely escaping electromagnetic emissions, the reader is referred to Chapter 7, which describes the phenomenology of Jovian radio emissions detected by Voyager.

8.2. Upstream waves and bow shock

During the approach to Jupiter two primary types of plasma waves, ion-acoustic-like waves and electron plasma oscillations were detected by the plasma-wave instrument in the solar wind upstream of the bow shock. A wideband frequency-time spectrogram illustrating the detailed structure of a series of ion-acoustic wave bursts observed upstream of Jupiter at a radial distance of 198.5 R_J is shown in Figure 8.1. Typically, these waves consist of an intense narrowband emission in the frequency range from about 500 Hz to 2 kHz. The center frequency of the emission varies erratically, sometimes remaining nearly constant for several seconds, as near the beginning of the spectrogram, and at other times displaying an inverted U-shaped feature lasting only 1 or 2 s, as near the end of the spectrogram. Typical broadband electric-field amplitudes for these bursts range from about 10 to 30 μV/m.

Comparisons of the Voyager spectrograms with comparable spectrograms obtained by Earth-orbiting spacecraft [Kurth, Gurnett, and Scarf, 1979] provide a strong indica-

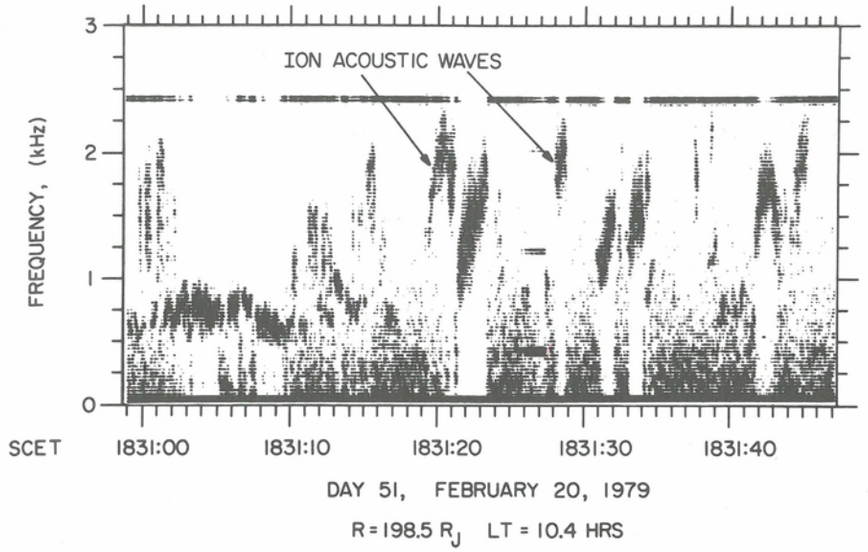

Fig. 8.1. A wideband frequency-time spectrogram of ion-acoustic-like waves detected upstream of the bow shock at Jupiter by the Voyager 1 Plasma Wave Experiment. Similar waves are observed upstream of the Earth's magnetosphere and are produced by ion beams streaming into the solar wind from the bow shock.

tion that these waves are essentially identical to the waves identified by Gurnett and Frank [1978a] as ion-acoustic waves upstream of the Earth's bow shock. These waves were first observed by Scarf et al. [1970] and are known to be closely correlated with suprathermal protons streaming into the solar wind from the Earth's bow shock. The identification of the mode of propagation as the ion-acoustic mode by Gurnett and Frank [1978a] is based on several factors including (1) the wavelength, which extends down to only a few times the Debye length λ_D, (2) the polarization, which is linear and approximately parallel to the static magnetic field, and (3) the absence of a wave magnetic field, which indicates that the wave is electrostatic. These conclusions have recently been further confirmed and amplified by Anderson et al. [1981]. The short wavelengths imply that the frequency observed in the spacecraft frame of reference is mainly determined by Doppler shifts, so that

$$f = (V_s/\lambda) \cos \theta_{kv} \tag{8.1}$$

where V_s is the solar wind velocity, λ is the wavelength, and θ_{kv} is the angle between the propagation vector and the solar wind velocity. The large solar wind Doppler shift explains why the observed frequency extends well above the ion plasma frequency ($f_{pi} \simeq 100$ Hz at 5 AU), which is the upper frequency limit of the ion-acoustic mode in the rest frame of the plasma. Although all the present indications support the identification of these waves as ion-acoustic waves, a complete theory for the generation of these waves by the upstream ion beams has not yet been established. For this reason, Gary [1978] and others have referred to these waves as ion-acoustic-like waves, because the mode involved may be a beam-related mode that is formally distinct from the ion-acoustic mode, although it has many similar characteristics. It is also interesting to note that these ion-acousticlike waves are also observed in the solar wind at locations remote from any possible bow-shock effects [Gurnett and Anderson, 1977], so that the conditions required for their generation are not uniquely related to magneto-

spheric bow shock interactions. In addition, Kurth, Gurnett, and Scarf [1979] have shown that the same type of ion-acousticlike waves are observed ahead of interplanetary shocks.

The second principal type of plasma wave observed upstream of the bow shock consists of electron plasma oscillations, also sometimes called Langmuir waves. A wideband frequency-time spectrogram of electron-plasma oscillations detected at a radial distance of 82.3 R_J is shown in Figure 8.2. The primary Langmuir wave emission is evident as the narrow dark line at about 5 kHz. This frequency corresponds very closely to the local electron plasma frequency, f_{pe}, in the solar wind. Because the wavelength of the main emission is believed to be very long, $\lambda \simeq 1$ to 10 km, the Doppler shift of the primary emission line is quite small, $\Delta f \simeq 100$ Hz [Gurnett et al., 1981a]. In addition to the primary Langmuir wave emission, many impulsive secondary emissions can also be seen extending upward and downward in frequency from the primary emission line. These upper and lower sideband emissions are believed to be short wavelength Langmuir waves produced from the primary "pump" wave by non-linear parametric interactions. The frequency shift is due to a combination of the Doppler shift, which can be of either sign depending on the direction of propagation, and the intrinsic frequency shift caused by the wave number dependence in the Langmuir wave dispersion relation,

$$f^2 = f_{pe}^2 (1 + 3k^2 \lambda_D^2) \tag{8.2}$$

which always produces an upward frequency shift. Detailed analyses by Gurnett et al. [1981a] indicate that the sideband emissions have wave numbers of approximately $k\lambda_D \simeq 0.15$, whereas the primary pump wave has a wave number about a factor of 10 smaller, with $k_0\lambda_D \simeq 0.015$. The electric field strength of the primary emission line is typically in the range from about 10 to 100 μV/m and tends to increase in intensity as the spacecraft approaches the shock. Because of the bursty character of the sideband emissions, it has not been possible to accurately determine the intensity of these emissions. However, it is believed that the sideband bursts are considerably more intense than the main emission line because the bursts frequently saturate the wideband receiver. The short duration of the sideband bursts, sometimes lasting only a few milliseconds, has led to the suggestion that these bursts may be so intense that nonlinear effects cause the wave to intensify and collapse into discrete spatial structures with scale sizes of only a few Debye lengths [Gurnett et al., 1981a]. Such collapsed spatial structures are called solitons. For a review of the theory of Langmuir wave solitons, see Nicholson et al. [1978].

Comparisons with plasma wave observations near the Earth show that the electron plasma oscillations detected by Voyager have characteristics very similar to electron-plasma oscillations observed upstream of the Earth's bow shock, thereby suggesting that they are generated by essentially the same mechanism. Scarf et al. [1971] showed that the electron plasma oscillations observed upstream of the Earth's bow shock are correlated with the occurrence of beams of nonthermal electrons arriving from the bow shock. Further studies by Gurnett and Frank [1975] and Filbert and Kellogg [1979] showed that the plasma oscillations occur when the beam of nonthermal electrons produces a double hump in the electron distribution function. The double hump arises because of time-of-flight considerations involving the propagation of the electron beam from the bow shock to the spacecraft. These considerations all strongly suggest that the electron plasma oscillations upstream of the terrestrial and Jovian bow shock are produced by the classic electrostatic two-stream instability that occurs when a superthermal electron beam streams through a stationary background

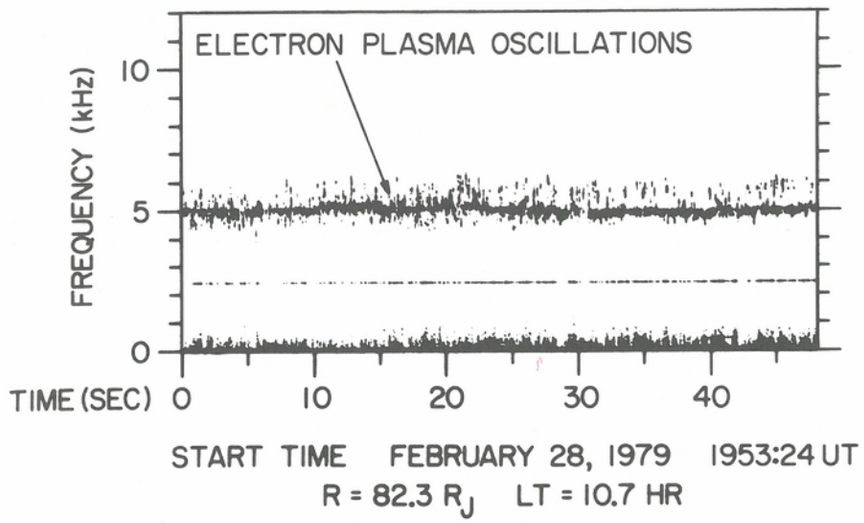

Fig. 8.2. A wideband frequency–time spectrogram of Langmuir waves detected by Voyager 1 in the solar wind upstream of the Jovian bow shock. These waves are generated by low energy, 1–10 keV, electrons streaming into the solar wind from the bow shock. Note the fine structure, which is believed to arise from nonlinear parametric decay processes.

plasma [Stix, 1962]. The principal scientific questions that remain have to do mainly with the nonlinear beam stabilization processes that prevent the instability from completely disrupting the beam [Papadapoulos, Goldstein, and Smith, 1974]. Both the terrestrial and Jovian observations show that the electron beam that generates the plasma oscillations can propagate large distances ($>10^5$ km) through the solar wind plasma. The nonlinear parametric interactions and soliton collapse effects observed upstream of the Jovian bow shock provide the first space-plasma measurements of the nonlinear effects involved in the beam stabilization process.

At the Jovian bow shock, an abrupt burst of low frequency electric field noise occurs with characteristics similar to the terrestrial bow shock. Because of the fluctuations in the position of the bow shock, a total of at least 23 shock crossings were observed during the inbound and outbound passes of Voyagers 1 and 2. These shocks display a variety of characteristics, ranging from narrow laminar structures characteristic of quasiperpendicular shocks to extended structures characteristic of quasiparallel shocks. The frequency-time spectrogram of one shock for which we obtained exceptionally good wideband electric field spectrum measurements is shown in Figure 8.3. The abrupt increase in both the intensity and frequency of the low-frequency electric field noise at the shock is clearly evident about 39 s after the start of the spectrogram. At peak intensity, the broadband electric-field strength is about 1.3 mV/m. This electric field noise is thought to be responsible for the ion and electron heating that takes place at the shock. Inspection of Figure 8.3 also shows that the main shock disturbance is preceded by a low-frequency precursor that starts about 10 s before the shock and gradually rises in frequency and intensity as the shock approaches. The onset of the low frequency precursor occurs at about the same time that the intensity of the upstream electron plasma oscillations starts to decrease. The rapid decrease in the electron plasma oscillation intensities just ahead of the shock is believed to be due to an increase in Landau damping as the electron temperature increases just ahead of the

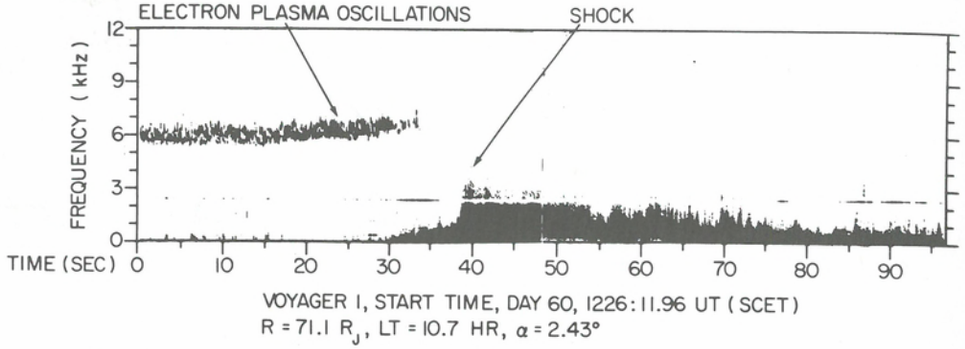

Fig. 8.3. A wideband spectrogram of the electric field turbulence at one of several bow-shock crossings observed upstream of the Jovian magnetosphere. Note the abrupt termination of the electron plasma oscillations just ahead of the shock and the ramp of low frequency noise starting about 10 s ahead of the shock. The abrupt burst of electric field noise at the shock is probably ion-acoustic or Buneman-mode turbulence driven by currents at the shock front. The electric field turbulence extends for several minutes into the region downstream of the shock [from Scarf, Gurnett, and Kurth, 1979].

shock. Downstream of the shock, the electric field turbulence decays rapidly in intensity and is no longer detectable a few minutes after the shock crossing. For further details of this shock, see Scarf, Gurnett, and Kurth [1979].

To compare the electric-field turbulence at the terrestrial and Jovian bow shock, the left panel of Figure 8.4 shows a composite summary of the electric field spectra (one 4 s scan at the time of maximum intensity) for nine bow shock crossings detected during the dayside inbound passes of Voyagers 1 and 2. The corresponding panel on the right shows a composite summary of the electric field spectra from 36 terrestrial bow shock crossings selected at random from the IMP 6 data [Rodriguez and Gurnett, 1975]. As can be seen, the general range of electric field spectral densities in the shock are similar at Jupiter and Earth. In both cases the spectrum shows a broad peak at low frequencies, with a rapid decrease in intensity as the frequency approaches the electron plasma frequency. For comparison, the nominal electron plasma frequencies in the solar wind are indicated in Figure 8.4 at Jupiter and Earth. It is evident that the electric-field spectrum at Jupiter is shifted downward in frequency compared to the Earth, approximately in proportion to the electron plasma frequency in the solar wind. Because of the possibility of large Doppler shifts, it is not known whether the upper cutoff near the plasma frequency is directly related to f_{pe} or is an upper limit on the Doppler shift, which also varies in direct proportion to f_{pe} because of the density dependence of the minimum wavelength, $\lambda_{min} = 2\pi\lambda_D$, [Gurnett and Anderson, 1977]. According to long standing ideas [Fredricks et al., 1968; Tidman and Krall, 1971; Greenstadt and Fredricks, 1979] the electric-field turbulence is thought to consist of ion-acoustic or Buneman mode waves driven by currents in the shock front. Although the main instability takes place near the ion plasma frequency, Doppler shifts caused by the solar wind motion tend to shift the frequency upward as detected in the spacecraft frame of reference. The broad frequency spectrum presumably arises because of the wide range of wave numbers and wave normal directions that are present in the electrostatic turbulence.

Although the general features of the bow shock turbulence appear to be quite similar at Earth and Jupiter, several important differences are evident. As can be seen from Figure 8.4, the rapid monotonic rise in the electric field intensities at low frequencies, less than 100 Hz, is not as evident at Jupiter. In the Earth's bow shock this low-

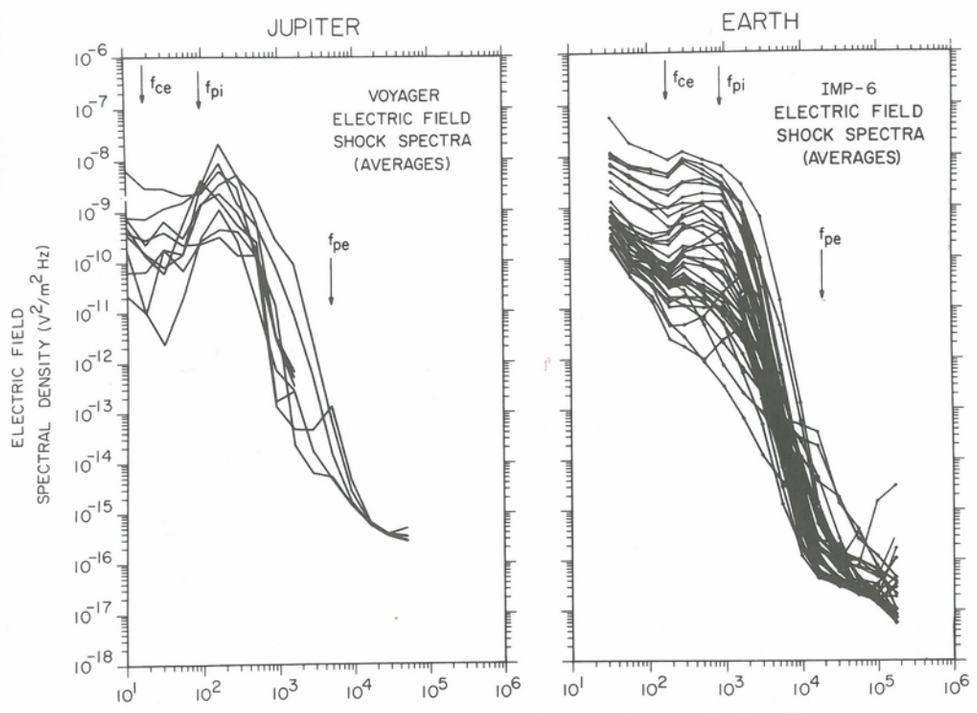

Fig. 8.4. A comparison of bow-shock electric field spectra at Earth and Jupiter. The peak electric field intensities are quite similar; however, the frequencies at the Jovian shocks appear to be shifted downward somewhat compared to the terrestrial shocks, probably owing to the lower solar wind plasma frequency. A notable difference at Jupiter is the near absence of the whistler-mode component that is apparent at low frequencies in the terrestrial shock spectra [from Rodriguez and Gurnett, 1975].

frequency electric field noise is believed to be due to whistler-mode waves generated in the shock [Rodriguez and Gurnett, 1975; Greenstadt et al., 1981]. It appears, therefore, that whistler-mode noise may not be as important in the Jovian bow shock as in the Earth's bow shock. This difference may be related to the average magnetic field direction, which tends to be more nearly perpendicular to the solar wind flow at Jupiter. It is interesting to note that at Venus, where the nominal magnetic field direction is even more radial than at Earth, the low-frequency noise is elevated with respect to the terrestrial case [Scarf et al., 1980]. However, the magnetic field direction is not the only important solar-wind characteristic that changes significantly with heliocentric radial distance, and it is possible that variations in the plasma β-value ($\beta = 8\pi NkT/B^2$), the thermal anisotropy ($T_\parallel/T_\perp$) or other parameters could produce the observed changes in the low-frequency turbulence spectrum.

Another feature of the Jovian bow shock interaction that seems to be different than the Earth is the turbulence downstream of the shock. At Earth, the entire magnetosheath region downstream of the shock is very turbulent, with intense electrostatic turbulence extending several hundred thousand kilometers into the downstream region [Rodriguez, 1979]. At Jupiter the electrostatic turbulence apparently decays in intensity very rapidly in the region downstream of the shock. Consequently, the electric-field noise levels are very low throughout most of the magnetosheath. The reason for this large difference in the magnetosheath electrostatic turbulence levels is not presently understood.

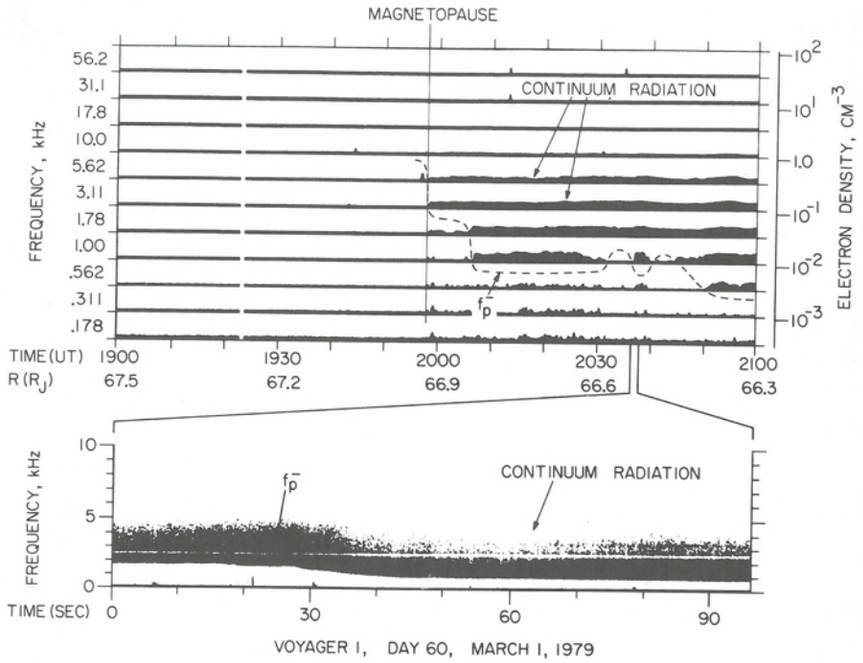

Fig. 8.5. A Voyager 1 magnetopause crossing that shows the electromagnetic continuum radiation trapped in the low density cavity inside the magnetosphere. The sharp low frequency cutoff of the continuum radiation is at the local electron plasma frequency, which gives a direct measurement of the electron concentration.

8.3. Trapped continuum radiation

Proceeding inward closer to Jupiter the next principal type of plasma wave detected was continuum radiation trapped in the low density cavity of the magnetosphere. Figure 8.5 shows the initial magnetopause crossing at which this radiation was first discovered. Immediately after the magnetopause crossing at 1957 UT, a relatively steady level of electric field noise is evident at frequencies below about 10 kHz. This noise has a relatively smooth spectrum with a sharp low-frequency cutoff. A wideband spectrogram showing the extremely sharp low-frequency cutoff is shown in the bottom panel of Figure 8.5. On the basis of similar observations of the same radiation in the Earth's magnetosphere [Gurnett and Shaw, 1973] the low frequency cutoff of the continuum radiation is identified as the local electron plasma frequency. Because the electron plasma frequency is determined by the electron concentration, $f_{pe} \simeq 9\,(n_e)^{1/2}$, where n_e is in units of cm^{-3} and f_{pe} is in kHz, the electron concentration can be inferred from this cutoff. The inferred electron concentration variations are indicated by the dashed lines in the top panel, with the electron concentration scale shown to the right. Because of the relatively coarse frequency resolution of the 16-channel spectrum analyzer, the electron concentration is determined only to within a factor of three using these data. More accurate electron concentration measurements, to an accuracy of a few percent, can be obtained from the wideband spectrograms, as in the bottom panel. However, these high-resolution wideband measurements are only available at isolated points. A complete survey of all the electron concentration measurements obtained using this technique is given by Gurnett et al. [1981b].

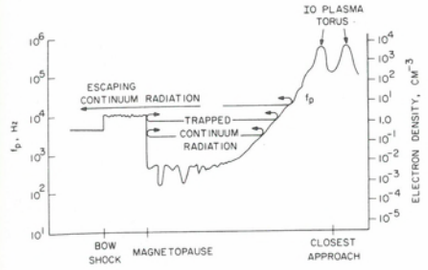

Fig. 8.6. A schematic illustration showing the reflection and trapping of continuum radiation in the low-density cavity inside the magnetosphere.

The mechanism by which the continuum radiation is trapped in the magnetosphere is illustrated in Figure 8.6. Because the electron concentration in the magnetosphere is much lower than in the solar wind, a large region exists where electromagnetic radiation can be trapped within the magnetosphere at frequencies below the solar-wind plasma frequency. Because the plasma is essentially collisionless, the reflection coefficient at the boundaries of the cavity is very close to unity, so that a large number of reflections can occur. The low density cavity not only includes the region around the nose of the magnetosphere but also extends into the tail of the magnetosphere, extending several AU or more downstream of Jupiter [Scarf, et al., 1981]. Because many reflections can occur, the trapped continuum radiation fills essentially the entire magnetospheric cavity. Representative ray paths illustrating the multiple reflections that can occur are shown in Figure 8.7. Because the reflection point at a specific frequency depends on the electron concentration distribution in the magnetosphere, the region accessible to the radiation varies with the wave frequency. At frequencies below the maximum plasma frequency in the distant plasma sheet, which is about 500 Hz, the radiation is trapped between the magnetopause and plasma sheet as shown in Figure 8.7. At higher frequencies, but still below the solar-wind plasma frequency, the radiation penetrates through the plasma sheet and is reflected at the magnetopause. At even higher frequencies, above the magnetosheath and solar-wind plasma frequency, the continuum radiation can escape freely from the magnetosphere as illustrated in Figure 8.6. Escaping continuum radiation, at frequencies above the solar wind plasma frequency, was detected in the solar wind during both the inbound and outbound passes of Voyagers 1 and 2. In this frequency range the continuum radiation changes into a discrete spectrum consisting of many closely spaced narrowband emissions. The pervasive character of the trapped continuum radiation is further demonstrated by the close similarity of the radiation spectrum at widely separated points in the magnetosphere. The left-hand panel of Figure 8.8, for example, shows three representative power spectra from the dayside plasma sheet, the nightside plasma sheet, and the tail lobe regions of the magnetosphere. With the exception of the low-frequency cutoff, which depends on the local plasma frequency, the high frequency parts of spectra are essentially identical in all three regions. The spectrum of the radiation is very steep, $\sim f^{-4}$, and extends down to extremely low frequencies, $\lesssim 20$ Hz, in the tail lobe, implying electron concentrations less than 3×10^{-6} cm^{-3} in this region.

Comparisons of the Jovian and terrestrial continuum radiation provide strong evidence that essentially the same type of radiation is present at both planets. In both cases the spectrum of the trapped component is relatively smooth and steady, and a sharp low-frequency cutoff is present at the local electron plasma frequency. For comparison, the right-hand panel of Figure 8.8 shows some representative continuum radiation spectra in the Earth's magnetosphere. As can be seen, the general shape of the terrestrial continuum radiation spectrum is very similar to the Jovian continuum radia-

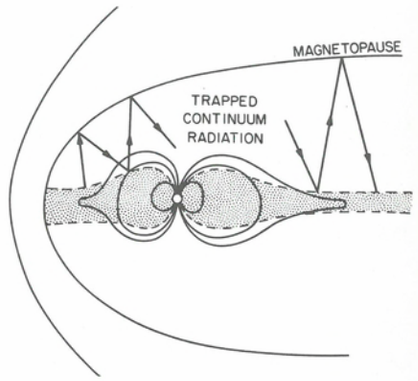

Fig. 8.7. Typical ray paths for the trapped continuum radiation showing that the radiation can propagate long distances in the magnetospheric cavity. At sufficiently low frequencies, the radiation is trapped as shown between the magnetopause and the plasma sheet, whereas at somewhat higher frequencies the radiation can penetrate through the plasma sheet thereby allowing propagation between the northern and southern tail lobes.

tion spectrum. However, at Jupiter, the intensities are generally higher and the radiation extends down to lower frequencies, mainly because of the much lower plasma concentrations in the Jovian magnetotail. The main argument that the continuum radiation at Jupiter consists of electromagnetic radiation comes from comparison with terrestrial observation. Because the Voyager instrumentation does not include a magnetic antenna, the electromagnetic character of the noise cannot be directly confirmed at Jupiter. However, magnetic field measurements with the IMP 6 spacecraft in the Earth's magnetosphere [Gurnett and Shaw, 1973] show that the continuum radiation consists of electromagnetic radiation with $E \simeq cB$. Terrestrial observations also demonstrate [Gurnett, 1975; Kurth, Gurnett, and Anderson, 1981] that the continuum radiation consists of both a trapped and escaping component, with the spectrum changing to a series of narrowband emissions above the solar wind plasma frequency very similar to the Jovian observations.

Two basic mechanisms have been proposed for generating the continuum radiation observed in planetary magnetospheres. First, Frankel [1973] suggested that continuum radiation escaping from the terrestrial magnetosphere may be generated by synchrotron radiation from energetic electrons; and second, Gurnett [1975] and Gurnett and Frank [1976] suggested on the basis of observations obtained in the Earth's magnetosphere that the continuum radiation is generated by mode-coupling from electrostatic waves near the local electron plasma frequency. The electrostatic mode-coupling mechanism has been further refined and discussed by a number of investigators including Jones [1976], Kurth et al. [1979b], Kurth, Gurnett, and Anderson [1981], and Melrose [1981], and it now appears to be the favored mechanism for generating the continuum radiation. The specific electrostatic modes involved in the generation of the continuum radiation are discussed in the next section.

Recently, Barbosa [1981] has addressed the question of how the narrowband emission generated by a mode-coupling process could be converted into a nearly continuous spectrum. Although the trapped continuum radiation spectrum is usually relatively smooth and continuous, as in Figure 8.5, occasionally narrowband features are evident [see Figure 8 from Gurnett and Shaw, 1973; or Figure 3 from Gurnett, Kurth, and Scarf, 1979a]. This narrowband structure strongly suggests that the radiation originates as a superposition of many distinct narrowband emissions. Barbosa's mechanism for spreading the spectrum of the trapped continuum radiation involves the Doppler shift that occurs each time the radiation reflects from the magnetopause boundary. Because of the random fluctuations in the velocity of the magnetopause in response to variations in the solar wind pressure, this mechanism converts the narrowband emissions generated by the mode-coupling process to an essentially continuous spectrum at frequencies below the solar wind plasma frequency. At frequencies above the solar wind plasma frequency reflections do not occur at the magnetopause, which explains why the spectrum switches from a continuum to series of narrowband emissions at this frequency.

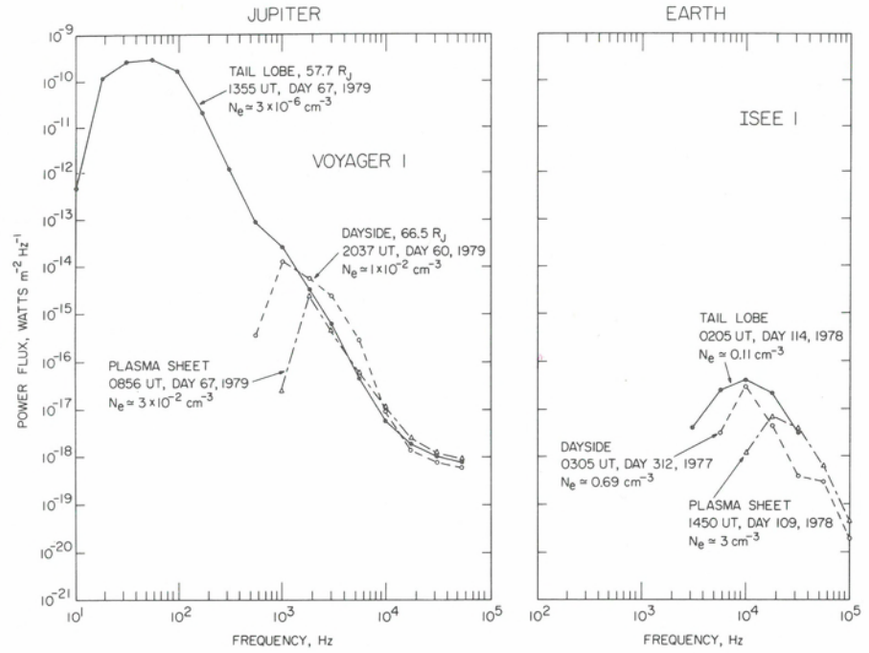

Fig. 8.8. A comparison of continuum radiation spectra in the Jovian and terrestrial magnetospheres. Although the overall features are quite similar, the continuum radiation extends to much lower frequencies at Jupiter and is much more intense, apparently owing to the steep spectrum and extremely low electron concentrations in the Jovian tail lobes. Note that the spectral intensities are similar in the upper part of the frequency range.

8.4. Upper hybrid and electron cyclotron waves

Within the Jovian magnetosphere, numerous narrowband electrostatic emissions were detected by both Voyagers 1 and 2 over a wide range of radial distances. On the basis of similar observations in the Earth's magnetosphere these emissions are identified as being of two related types: upper-hybrid resonance waves at $f_{UHR} = (f_{ce}^2 + f_{pe}^2)$, and electron cyclotron waves near half-integral harmonics of the electron cyclotron frequency, $(n + 1/2)\, f_{ce}$. These two types of waves are shown circled in Figure 8.9. The electron cyclotron waves occur just above the electron cyclotron frequency, at about $3\, f_{ce}/2$ and $5\, f_{ce}/2$, and the upper-hybrid resonance waves occur at slightly higher frequencies, a specific example being the isolated intense emission in the 31.1-kHz channel at about 0000 UT on March 5. As can be seen from the magnetic latitude given in the lower panel of Figure 8.9, the upper-hybrid and electron cyclotron emissions occur simultaneously, however, occasionally only one of the two types may be present at a time. The intensities of the upper-hybrid and electron cyclotron waves vary over a

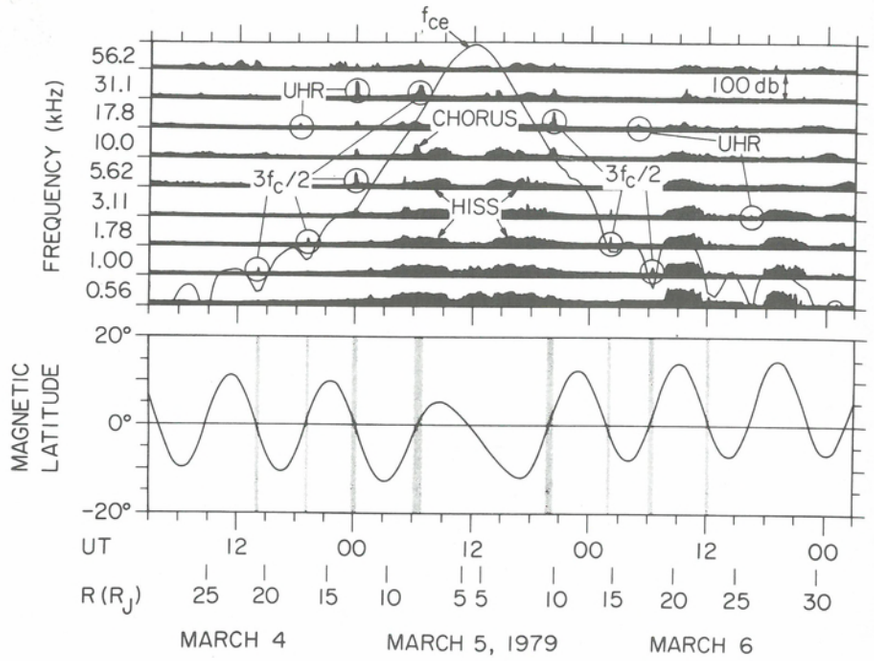

Fig. 8.9. The 16 channel spectrum analyzer data for the Voyager 1 pass by Jupiter showing the occurrence of low order, 3 $f_{ce}/2$ and 5 $f_{ce}/2$, electron cyclotron emissions and *UHR* emissions near the equatorial plane. Whistler-mode chorus and hiss emissions are also evident in the inner region of the magnetosphere [from Kurth et al., 1980b].

wide range, from only a few microvolts per meter to a few millivolts per meter. Generally, the most intense emissions occurred in the inner magnetosphere, near closest approach.

A high-resolution wideband spectrogram illustrating the detailed frequency-time structure of the upper-hybrid waves is shown in Figure 8.10. As can be seen, the upper-hybrid waves consist of intense narrowband emissions near the low-frequency cutoff of the trapped continuum radiation, at approximately f_{pe}. The frequency of these emissions, near the low-frequency cutoff of the continuum radiation, is consistent with the fact that the electron cyclotron frequency is much less than the electron plasma frequency, which places the upper-hybrid resonance frequency very close to the plasma frequency, $f_{UHR} \simeq f_{pe}$. A striking characteristic of the upper-hybrid resonance emissions shown in Figure 8.10 is the fact that the emission frequency is not continuous, but rather consists of a series of discrete lines that have a frequency spacing corresponding to the local electron cyclotron frequency. Careful comparisons indicate that the individual emission lines occur when $(n + 1/2)\, f_{ce} \simeq f_{UHR}$. As can be seen from the continuum radiation cutoff, the variations in plasma concentration cause the upper-hybrid resonance frequency to sweep across successive half-integral harmonics of the electron cyclotron frequency. Intense upper-hybrid emissions occur whenever the plasma concentration is such that the condition $(n + 1/2)\, f_{ce} \simeq f_{UHR}$ is satisfied.

A somewhat similar relationship between the upper-hybrid emissions and the half-integral electron cyclotron harmonics is evident in the measurements from the planetary radio astronomy experiment near closest approach [Warwick et al., 1979a]. Figure 8.11 summarizes the frequency structure of the upper-hybrid and electron cyclotron

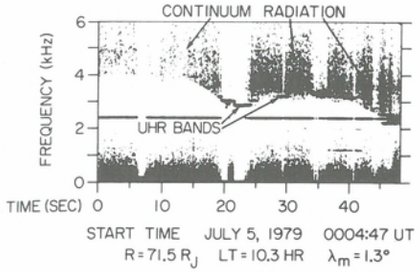

Fig. 8.10. A wideband spectrogram showing the details of the upper-hybrid resonance emissions. Note that this emission is not a continuous band, but consists of a series of discrete emissions that occur near half-integral harmonics of the electron cyclotron frequency, when $(n + 1/2)\, f_{ce} \simeq f_{UHR}$.

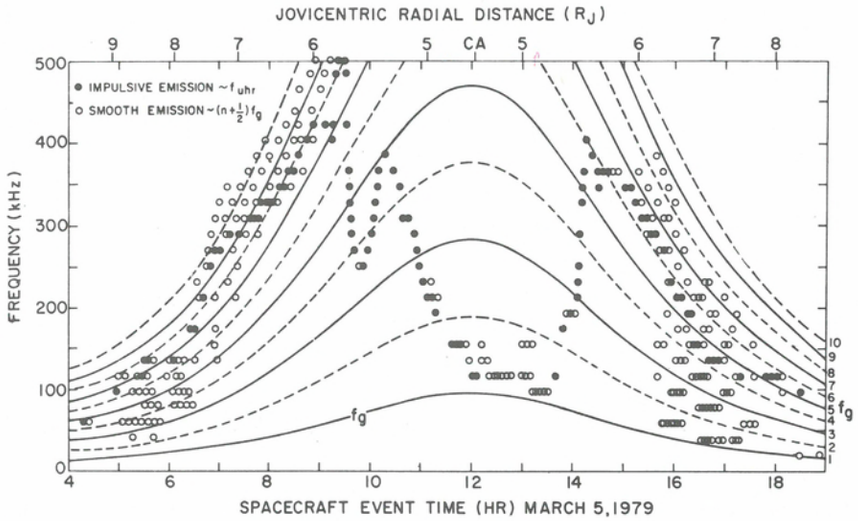

Fig. 8.11. A summary of the frequencies of upper-hybrid and electron cyclotron emissions observed by the planetary radio astronomy experiment during the pass through the Io plasma torus on March 5, 1979 [Birmingham et al., 1981]. The black circles signify impulsive emissions near f_{UHR} while the open circles denote smooth emissions near $(n + 1/2)\, f_{ce}$.

waves observed during the pass through the Io torus [Birmingham et al., 1981]. Two types of emissions can be identified in this region: relatively intense impulsive emissions at f_{UHR}, and somewhat weaker smooth emissions at $(n + 1/2)\, f_{ce}$. The impulsive emissions at f_{UHR} are probably analogous to the upper-hybrid waves shown in Figure 8.10, although the splitting into discrete lines is not as evident, possibly because of the more limited frequency resolution. This upper-hybrid resonance emission was used by Warwick et al. [1979a] to obtain the electron concentration profile shown in Figure 8.12. The two broad peaks in the concentration profile at about 0930 and 1430 UT correspond to the inbound and outbound passes through the Io torus. The smooth emissions which tend to occur at $(n + 1/2)\, f_{ce}$ in Figure 8.10 appear to be yet another type of electron cyclotron emission. These emissions are characterized by relatively smooth diffuse frequency structure that contrasts sharply with the more impulsive low-order electron cyclotron emission observed farther out in the magnetosphere. These smooth diffuse bands also tend to reach maximum intensity near f_{UHR}, rather than at the low order half-integral harmonics.

Upper-hybrid resonance emissions displaying somewhat similar quantitized frequency structure at half-integral harmonics of the electron cyclotron frequency have

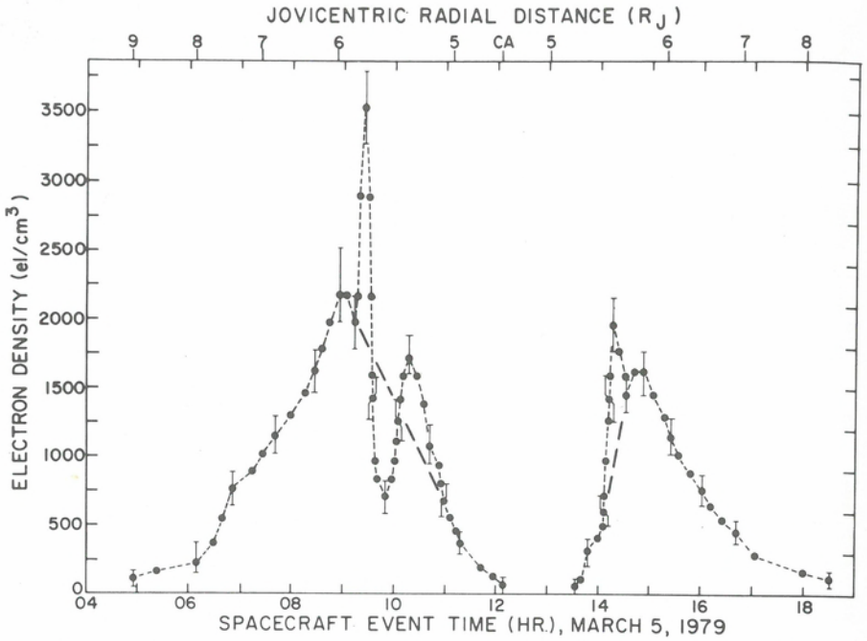

Fig. 8.12. The electron concentration profile obtained from the upper-hybrid emissions in Figure 11. The two broad peaks correspond to the inbound and outbound passes through the Io torus. The dashed line indicates a possible smoothing according to Cummings et al. [1980]. The peaks farthest left and farthest right correspond to the Io L-shell.

also been observed in the Earth's magnetosphere [Shaw and Gurnett, 1975] and have been discussed in detail by Kurth et al. [1979b]. The occurrence of half-integral cyclotron harmonic effects at the upper-hybrid resonance demonstrates that these emissions are related to a general class of electron cyclotron emissions at $(n + 1/2)\, f_{ce}$ which were first observed near $3\, f_{ce}/2$ and $5\, f_{ce}/2$ in the Earth's magnetosphere by Kennel et al. [1970]. When the electron plasma frequency is well above the cyclotron frequency, $f_{pe}/f_{ce} >> 1$, these emissions split into two well-defined groups consisting of one prominent emission line near f_{UHR}, and a set of low order lines: at $(n + 1/2)\, f_{ce}$, where n usually does not extend above 2 or 3. These emissions have been extensively studied in the Earth's magnetosphere by many investigators, including Fredricks and Scarf [1973], Scarf et al. [1973], Shaw and Gurnett [1975], Christiansen et al. [1978], and Kurth et al. [1979b]. Relatively smooth diffuse electron cyclotron emissions possibly related to the smooth $(n + 1/2)\, f_{ce}$ emissions in the Io torus have also been observed in the Earth's magnetosphere [Shaw and Gurnett, 1975; Hubbard and Birmingham, 1978]. Thus, a wide body of research exists in the Earth's magnetosphere that is directly applicable to the interpretation of the Jovian upper hybrid and electron cyclotron emissions.

Theoretical studies of the upper hybrid and electron cyclotron waves by numerous investigators including, for example, Fredricks [1971], Young, Callen, and McCune [1973], Hubbard and Birmingham [1978], Ashour-Abdalla and Kennel [1978a,b], and others have accounted for the main features of these emissions. Studies of the Harris dispersion relation [Harris, 1959] for electrostatic waves propagating in a hot plasma with a magnetic field indicate that the underlying requirement for instability is that the electron velocity distribution function must have a region of positive slope, $\partial f/\partial v_\perp > 0$, with respect to the component of velocity perpendicular to the magnetic

field, $v_\perp$. Cyclotron damping strongly attenuates waves near harmonics of the cyclotron frequency; therefore, the instability always occurs between an adjacent pair of cyclotron harmonics, but not necessarily at an exact half-integral harmonic. The identification of a given emission band with a specific half-integral harmonic is, therefore, only an identifying name, and does not necessarily imply that the emission frequency is exactly at the half-integral harmonic. The detailed growth rate of the electrostatic instability, and the number of unstable bands depends on a large number of parameters, the most important of which are the cold-to-hot electron concentration ratio and the cold electron temperature. Comparisons of wave intensities with electron distribution function measurements in the Earth's magnetosphere by Rönnmark et al. [1978] and Kurth et al. [1979b, 1980a] show good general agreement between theory and observations, although in some cases the source of the free energy is not completely obvious, possibly owing to modifications of the distribution function by the waves.

The existence of upper hybrid and electron cyclotron waves near the magnetic equator implies that electron distribution functions with a significant positive $\partial f/\partial v_\perp$ occur in this region of the Jovian magnetosphere. However, this relationship has not been confirmed with particle measurements, mainly because no electron measurements are available from Voyager with sufficient angular resolution in the proper energy range, 100 eV to 10 keV, to provide an adequate test of the theories involved.

The electrostatic upper-hybrid and electron cyclotron waves are possibly important for three processes in the Jovian magnetosphere. First, if the waves are sufficiently intense, they can cause pitch-angle diffusion and loss of energetic electrons trapped in the magnetic field; second, they can transfer energy from the hot to the cold electron population; and third, the upper-hybrid emission can couple to a free space electromagnetic mode and produce radio emissions. The possibility that low-order electron cyclotron waves could cause significant pitch-angle diffusion was first proposed by Fredricks and Scarf [1973] to explain the diffusion and energization of auroral electrons in the Earth's magnetosphere. Subsequent studies by Lyons [1974] demonstrate that electron cyclotron waves with intensities of 10 to 100 mV/m can account for strong pitch-angle diffusion of 1 to 20 keV electrons. Electron cyclotron waves with intensities approaching these levels have been reported by Scarf et al. [1973] in association with substorms in the Earth's magnetosphere. At Jupiter it is not known whether the amplitudes of the low order electron cyclotron waves are sufficiently large to produce significant pitch-angle diffusion effects. In the middle and outer regions of the magnetosphere the field strengths of the $3\, f_{ce}/2$ and $5\, f_{ce}/2$ emissions are very weak, only a few tens of μV/m; thus it is very unlikely that these waves produce important effects. Only in the inner magnetosphere, at radial distances less than about 15 R_J, do the electron cyclotron emissions reach intensities of a few millivolts per meter [Kurth et al., 1980b], which are possibly large enough to cause significant pitch-angle diffusion. In addition to pitch-angle scattering, studies of the nonlinear stabilization of the electron cyclotron harmonic emissions by Ashour-Abdalla and Kennel [1978b] suggest that these waves may cause a significant energy transfer from the hot to the cold electron populations. Such a heating process could, for example, be important in the Io plasma torus, which is known to consist of a relatively cool (10 eV) core component and a much more energetic (1 keV to 1 MeV) magnetospheric component.

The possibility that the upper-hybrid resonance emissions may play an important role in the generation of low frequency radio emissions has been suggested by a number of authors. In an early study of the terrestrial continuum radiation, Gurnett [1975] presented radial intensity profiles that strongly suggested that the continuum radiation originates from intense electrostatic noise bands near the local electron plasma frequency. Jones [1976] later suggested a specific mechanism for converting the electro-

static noise to electromagnetic radiation. Recently, after reviewing a number of mechanisms for generating the continuum radiation at both Jupiter and Earth, Melrose [1981] concluded that the most likely process for generating the continuum radiation involves a nonlinear interaction between the upper-hybrid emissions and a yet unidentified low-frequency mode. Strong evidence for the importance of the upper-hybrid emission as a source of both the trapped and escaping terrestrial continuum radiation has recently been presented by Kurth, Gurnett, and Anderson [1981]. Because the upper-hybrid emissions are observed over a wide range of radial distances inside the Jovian magnetosphere, including the Io torus [Warwick et al., 1979a; Birmingham et al., 1981], it seems quite likely that these emissions are involved in not only the generation of the trapped and escaping continuum radiation at Jupiter, but also other types of Jovian radio emissions at higher frequencies. A prime candidate is the narrowband Jovian kilometric radiation reported by Kaiser and Desch [1980], as this radiation appears to be generated near the equatorial plane in the outer regions of the Io plasma torus, which is a region known to include intense upper-hybrid resonance emissions.

8.5. Whistler-mode waves

Because several types of whistler-mode waves are observed in the Earth's magnetosphere, it was anticipated that some type of whistler-mode noise would be detected during the Voyager passes by Jupiter. In fact, four different types of whistler-mode signals were detected, each related to a type of whistler-mode noise present in the Earth's magnetosphere. The four types are (1) lightning-generated whistlers, (2) chorus, (3) hiss, and (4) auroral hiss.

Whistlers

One of the more striking results from the Voyager 1 plasma wave observations was the discovery of whistlers generated by lightning at Jupiter [Gurnett et al., 1979b]. The occurrence of lightning at Jupiter was not totally unanticipated; several investigators had already suggested that lightning was likely to be present in the Jovian atmosphere [Sagan et al., 1967; Bar-Nun, 1975]. Also, the possibility of detecting whistlers generated by lightning was considered in the overall planning and design of the plasma wave instrument [Scarf and Gurnett, 1977]. Nevertheless, when signals were detected from the Voyager 1 plasma wave instrument with the unmistakable whistling sounds characteristic of lightning-generated whistlers, it was regarded as a remarkable discovery because it was completely unknown whether the signals would be detectable given the long propagation paths involved (about 10 times longer than in the Earth's magnetopshere) and the largely unknown attenuation effects along the propagation path. During the pass by Jupiter, a total of 167 whistlers were identified in the Voyager wideband data. All of the whistlers detected were observed in a narrow range of L-shells near the inner edge of the Io plasma torus, from about 5.2 to 5.9 R_J and within $\pm 10°$ of the magnetic equator. Two of the best examples are shown in Figure 8.13. The characteristic decrease in the frequency with increasing time, which uniquely identifies these signals as whistlers, is clearly evident. Gurnett et al. [1979b] show that these signals fit the well-known equation

$$t - t_0 = D / \sqrt{f} \tag{8.3}$$

for the dispersion of whistlers first given by Eckersley [1935], where D is a constant called the dispersion. For the frequencies of interest the whistlers propagate approxi-

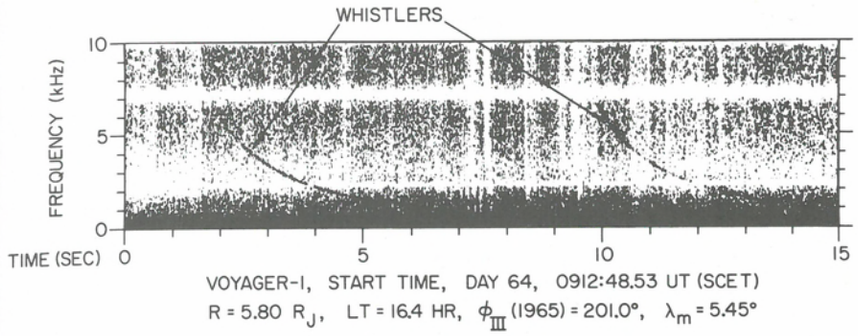

Fig. 8.13. A spectrogram of two long dispersion whistlers detected by Voyager 1 in the Io plasma torus. The whistler dispersion gives a weighted integral of the electron concentration along the propagation path.

mately along the magnetic field line from the base of the ionosphere to the spacecraft. The dispersion is proportional to the integral of $(n_e)^{1/2}/B$ along the ray path. The whistler dispersion varied over a large range, from $D \simeq 35$ to 570 s $Hz^{1/2}$. The small dispersion whistlers were observed near the edge of the torus and are believed to have reached the spacecraft without passing through the torus, whereas the large dispersion whistlers are believed to have passed through the torus. The very small dispersion of some of these whistlers, $D \simeq 50$ s $Hz^{1/2}$, demonstrates that the average electron concentration outside of the torus is small, only about 10 to 40 cm^{-3} along the $L = 6$ field line. For the whistlers that have passed through the Io plasma torus the dispersion provides a quantitative measure of its north–south thickness. Typical values for the torus thickness at $L \simeq 6$ from whistler dispersion measurements range from about 1.8 to 5.0 R_J [Gurnett et al., 1981b]. These thicknesses tend to be about a factor of 2 larger than the scale heights estimated from in situ plasma measurements [Bagenal, Sullivan, and Siscoe, 1980; Warwick et al., 1979a; Birmingham et al., 1981], presumably because the in situ plasma measurements do not include the contribution of light ions, such as protons, that would tend to increase the electron concentration away from the equator. Comparisons of the whistler dispersion with in situ measurements of heavy ion concentrations near the equatorial plane [Tokar et al., 1982] show that light ions tend to be the dominant constituent beyond about 2 R_J from the magnetic equator at $L \simeq 6$.

In addition to the scale height and electron concentration determinations, the Voyager whistler observations also place limits on the electron temperature in the torus because of the absence of appreciable Landau damping effects. As shown by Menietti and Gurnett [1980] the attenuation of whistlers due to Landau damping by hot electrons becomes unacceptably large if the electron temperature in the torus exceeds about (2 to 3) $\times$ 10^5 K. This upper limit is in good agreement with the results from the Voyager 1 ultraviolet spectrometer [Broadfoot et al., 1979] and plasma instrument [Scudder et al., 1981a], which indicate an average electron temperature of about 10^5 K.

Chorus and hiss

Two other types of whistler-mode waves called chorus and hiss were detected by both Voyagers 1 and 2 as the spacecraft passed through the Io torus. Both of these whistler-mode waves are spontaneously generated within the magnetosphere by interactions with energetic trapped electrons and are named after the corresponding phenomena in

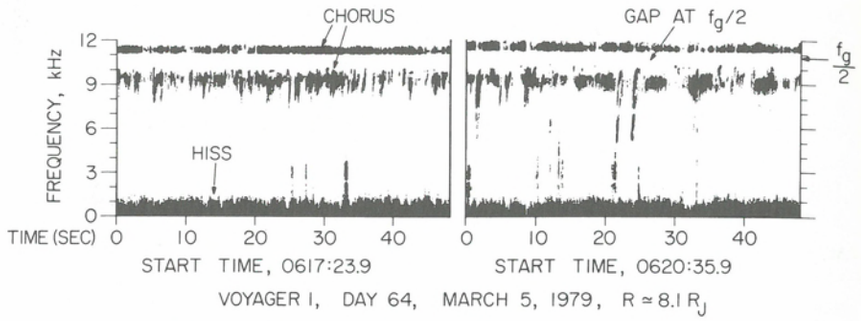

Fig. 8.14. Wideband frequency-time spectrograms of whistler-mode chorus and hiss observed in the Io plasma torus. The hiss consists of a relatively structureless emission below about 1 kHz, and the chorus consists of many discrete narrowband tones generally rising in frequency from about 8 to 12 kHz. Note the gap in the chorus spectrum at approximately $f_{ce}/2$.

the Earth's magnetosphere. The spectral characteristics of the chorus and hiss emissions are illustrated in Figure 8.14, which shows a wideband spectrum obtained from Voyager 1 at about 8.1 R_J. The chorus emissions occur from about 8 to 12 kHz and have a very complex spectral structure, typically consisting of short bursts that increase in frequency with increasing time. The hiss emissions, on the other hand, occur at much lower frequencies (below about 2 kHz) and are nearly structureless. A remarkable feature of the chorus emissions is the distinct gap in the spectrum at one-half the electron cyclotron frequency, $f_{ce}/2$. As can be seen from Figure 8.14, the low frequency cutoff of the upper portion of the chorus band is very close to $f_{ce}/2$. A well-defined gap occurs below this cutoff with a bandwidth of about 1 kHz. The chorus intensities are very similar above and below the gap. Within the gap, the intensities are at least 25 db below the peak intensities on either side. A qualitative difference is also evident in the detailed frequency-time structure above and below the gap; more rising tones and discrete features tend to occur in the lower band.

The spatial distribution of the chorus and hiss emissions detected by Voyager 1 can be seen in Figure 8.9. In the 16 channel spectrum analyzer data, the hiss corresponds to the very broadband emission extending from about 50 Hz to 10 kHz, with maximum intensity at a few hundred Hz [Scarf, Gurnett, and Kurth, 1979]. The hiss occurs from about 5.5 to 10 R_J on both the inbound and outbound legs, in the regions that correspond to the inbound and outbound passes through the Io plasma torus. The chorus emissions, on the other hand, occur only in a single frequency channel (10 kHz) for a brief period around 0615 UT on the inbound leg. This time corresponds to a crossing of the magnetic equator, thereby suggesting that the chorus may be confined to the vicinity of the magnetic equator. At maximum intensity the integrated broadband electric field strength of the hiss is a few millivolts per meter [Scarf, Gurnett, and Kurth, 1979]. The chorus is somewhat less intense than the hiss, and has a maximum broadband electric-field strength of about 0.26 mV/m [Coroniti et al., 1980a].

The whistler-mode hiss and chorus emissions observed at Jupiter have many remarkable similarities to hiss and chorus emissions observed in the Earth's magnetosphere. In fact, our identification of these waves as whistler-mode emissions rests mainly on these close similarities, because no magnetic field measurements are available from Voyager to prove conclusively that these waves are propagating in the whistler mode. In the Earth's magnetosphere whistler-mode emissions called chorus, with spectral characteristics similar to Jovian chorus have been observed for many years [Helliwell, 1965].

The earliest reports of ground-based very low frequency (VLF) radio observations with characteristics resembling what is now called chorus were by Preece [1894] and Burton and Broadman [1933]. The first systematic studies of the phenomena called chorus were conducted by Allcock and Martin [1956] and Allcock [1957] who coined the name "dawn chorus" because the received audio signals sounded like the chorus from a distant rookery at sunrise. After spacecraft measurements were available, it became apparent that the chorus emissions were due to a cyclotron resonance involving electrons trapped in the magnetic field. Tsurutani and Smith [1974] and Burtis and Helliwell [1976], for example, showed that the frequency of chorus emissions were related to the equatorial electron cyclotron frequency along the observer's L-shell. They also found that the chorus emissions frequently have a gap at one-half the electron cyclotron frequency. At about the same time, Russell, Holzer, and Smith [1969] identified another type of whistler-mode emission, later called plasmaspheric hiss by Thorne et al. [1973], which is oberved mainly inside the plasmasphere. In contrast to the chorus emissions, the plasmaspheric hiss has a relatively broad bandwidth with nearly constant intensity and occurs at frequencies well below the equatorial electron cyclotron frequency.

The first comprehensive theory of whistler-mode emissions, with applications to both chorus and hiss, was given by Kennel and Petschek [1966], who identified the electron pitch-angle anisotropy produced by the atmospheric loss cone as the free energy source for driving the whistler-mode instability. By utilizing the principal of conservation of angular momentum Brice [1964] showed that the generation of right-hand polarized whistler-mode waves leads to a reduction in the pitch angle of the resonant electrons. Therefore, the spontaneous emission of whistler-mode waves by a plasma tends to drive the resonant particles toward the loss cone, eventually leading to the loss of the particles. In the Earth's magnetosphere whistler-mode chorus and hiss emissions are now regarded as the primary mechanisms for the scattering and loss of energetic electrons trapped in the magnetosphere [Lyons, Thorne, and Kennel, 1972]. Similarly at Jupiter, chorus and hiss emissions are now thought to be mainly responsible for the scattering and loss of trapped electrons, with the hiss mainly interacting with high energies [Scarf et al., 1979a; Thorne and Tsurutani, 1979] and the chorus interacting with low energies [Coroniti et al., 1980a]. Figure 8.15 [from Coroniti et al., 1980a] for example, shows the resonant energies and pitch-angle scattering times for a typical chorus and hiss spectrum. As can be seen, the hiss tends to resonate with electron energies of a few hundred keV, and the chorus resonates with electrons of a few keV. The occurrence of hiss mainly in the high density region of the Io plasma torus is a consequence of the dependence of the whistler-mode resonance condition on the electron concentration [Kennel and Petschek, 1966]

$$E_{Res} = \frac{B^2}{2\mu_o n_e} \left(1 - \frac{f}{f_c}\right)^3 \frac{f_{ce}}{f} \tag{8.4}$$

where $B^2/2\mu_o n_e$ is an energy that characterizes the whistler-mode interaction. Higher electron number densities lower the resonant energy, thereby increasing the number of resonant electrons and the growth rate of the instability. Representative ray paths for hiss generated in the Io torus are illustrated in Figure 8.16, based on a similar sketch of hiss trapped in the Earth's plasmasphere by Thorne et al. [1973]. Because of the decreasing index of refraction away from the magnetic equator, whistler-mode waves tend to be reflected as soon as the wave frequency drops below the local lower-hybrid resonance frequency f_{LHR}. This lossless reflection process leads to repeated passes

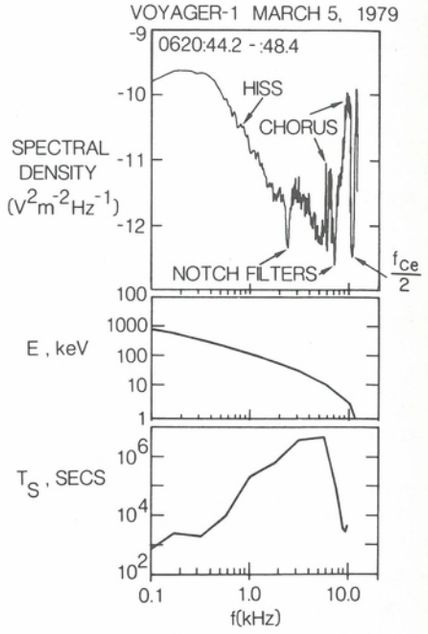

Fig. 8.15. A typical chorus and hiss spectrum and the corresponding electron resonance energies and scattering times for resonant whistler-mode interactions. The hiss scatters relatively energetic, few hundred keV, electrons whereas the chorus interacts with much lower-energy electrons, that have energies of a few keV [from Coroniti et al., 1980a].

of the whistler-mode wave through the torus and increases the time available for wave-particle interactions.

Although the Kennel–Petschek theory provides a general framework for understanding magnetospheric whistler-mode instabilities, many of the detailed characteristics of the whistler-mode emissions remain difficult to explain. This is particularly true for the chorus bursts, which display very complex frequency-time characteristics. Specific models for the frequency variation of the chorus emissions have, for example, been developed by Helliwell [1967] and Helliwell and Crystal [1973] to account for the nonlinear feedback between the whistler-mode waves and the resonant electrons. However, it is uncertain at present whether these models can account for the detailed temporal behavior of individual chorus bursts. Similarly, even though numerous theories have been proposed to explain the gap in the chorus spectrum at $f_{ce}/2$ [Tsurutani and Smith, 1974; Maeda, Smith, and Anderson, 1976; Burtis and Helliwell, 1976; Curtis, 1978] the exact explanation of this effect remains unresolved.

Auroral hiss

A fourth type of whistler-mode noise called auroral hiss was also observed during the Voyager 1 pass through the Io torus [Gurnett, Kurth, and Scarf, 1979b]. The name of this noise is derived from a type of whistler-mode noise commonly observed in the Earth's auroral zones in association with intense low-energy, 10 eV to 1 keV, auroral electron precipitation. The distinguishing characteristics of the terrestrial auroral hiss are that it has (1) a very broad bandwidth, and (2) a V-shaped low-frequency cutoff [Gurnett, 1966; McEwen and Barrington, 1967]. The upper frequency limit of the emission typically extends up to near the electron cyclotron frequency and the lowest frequency, near the point of the V, is near the local lower-hybrid resonance frequency $f_{LHR} \simeq (f_{ce} f_{ci})^{1/2}$.

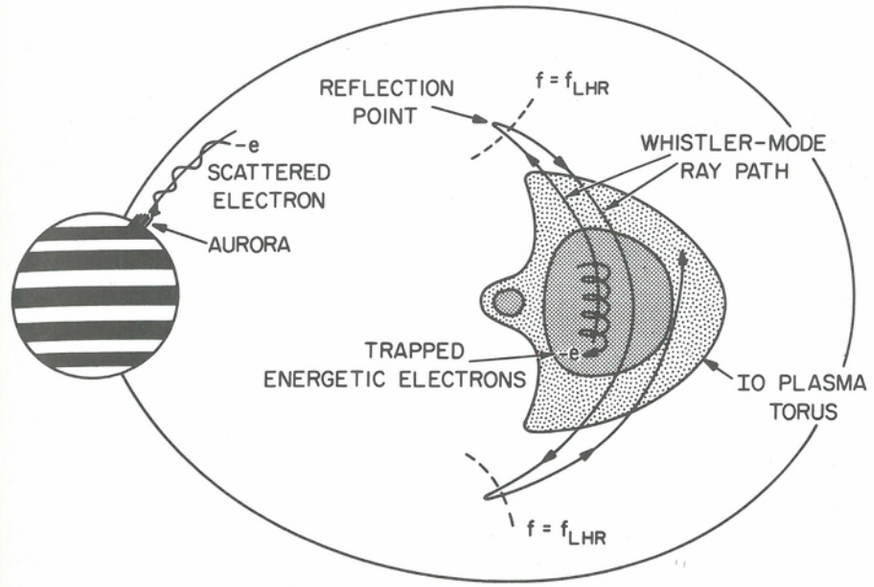

Fig. 8.16. A schematic illustration of typical whistler-mode ray paths for hiss and chorus interacting with trapped electrons in the Io plasma torus. The high plasma density in the torus lowers the resonance velocity and increases the whistler-mode growth rate. As the wave propagates away from the magnetic equator, the emissions are reflected as soon as the wave frequency drops below the local lower-hybrid resonance frequency, which returns the waves to the equatorial plane and further increases the time available for resonant interactions. This reflection process is sometimes compared with the mirrors in a laser, which cause repeated passes of the wave through the amplifying region.

A series of wideband frequency-time spectrograms illustrating the main features of the auroral hiss observed by Voyager 1 is shown in Figure 8.17. Because of the time sharing with the imaging system these spectrograms are not contiguous in time. Nevertheless, a broad band of noise can be identified during this period with a very well-defined low-frequency cuttoff that increases linearly in frequency with increasing time. The broadband character of this emission and the smoothly varying low-frequency cutoff provide an almost unmistakable identification of this emission as a V-shaped auroral hiss emission. This event occurs during the inbound pass through the inner edge of the torus, and another comparable emission is evident in the survey data during the outbound pass through the inner edge of the torus. Unfortunately, on both the inbound and outbound passes only one leg of the V can be distinguished, since the leg inside the torus tends to be obscured by the whistler-mode hiss emissions.

From measurements of the cutoff frequency as a function of time and a simple model for the whistler-mode ray paths, a rather accurate determination of the source position can be obtained. For the auroral hiss emissions, which are known to be propagating at angles close to the resonance cone, the limiting ray path angle with respect to the magnetic field is given by

$$\tan^2 \psi = \frac{f^2 - f_{LHR}^2}{f_{ce}^2} \tag{8.5}$$

Because higher frequency waves propagate at larger angles to the magnetic field, it is evident from the above equation that as the spacecraft approaches the field line

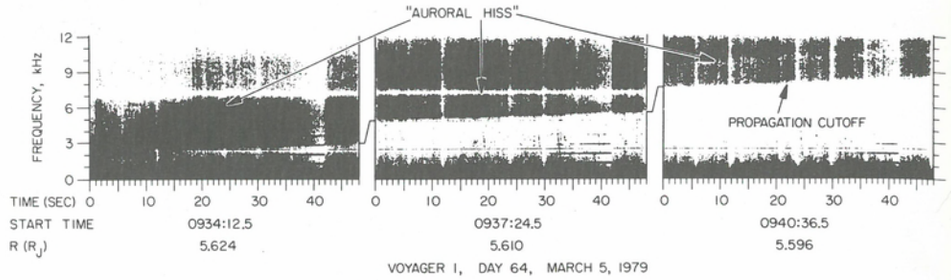

Fig. 8.17. A wideband spectrogram of auroral hiss observed at the inner edge of the torus. The auroral hiss is characterized by a broadband emission spectrum with a sharply defined low-frequency cutoff that increases linearly with time. The low frequency cutoff is produced by a frequency-dependent limiting angle for the whistler-mode ray path relative to the magnetic field [from Gurnett, Kurth, and Scarf, 1979b].

through the source the highest frequencies are detected first, with progressively lower and lower frequencies accessible as the spacecraft comes closer to the source field line. The sharp low-frequency cutoff of the auroral hiss indicates that the source terminates at a well-defined distance h upward along the magnetic field line. For the observed variation of the cutoff frequency in Figure 8.17, a best fit analysis of Equation 8.1 indicates that the spacecraft crossed the field line through the source at 0930 UT, and that the distance h to the source was 0.65 R_J [Gurnett, Kurth, and Scarf, 1979b]. Because the spacecraft was located close to the centrifugal equator at this time [Cummings, Dessler, and Hill, 1980], the source could be located either to the north or south of the equator. The approximate location of the auroral hiss source is shown in Figure 8.18 in relation to the electron number-density contours of the Io torus given by Bagenal, Sullivan, and Siscoe [1980]. It is evident from this comparison that the auroral hiss source is located almost exactly coincident with the sharp inner edge of the torus at $L = 5.6$. Because the auroral hiss was observed on both the inbound and outbound passes through the inner edge of the torus, it is concluded that the auroral hiss source extends longitudinally around the torus on the $L = 5.6$ L-shell at a distance of about 0.65 R_J from the equator.

The electric field intensity of the auroral hiss is small, only about 30 μV/m broadband intensity. Therefore, it is unlikely that the auroral hiss plays a significant role in the dynamics of the torus plasma. The principal importance of the auroral hiss is as an indicator of auroral processes occurring at the inner boundary of the torus. In the terrestrial auroral zone, the occurrence of auroral hiss is closely correlated with intense fluxes, 10^8 to 10^{10} electrons cm^{-2}, of low energy, 10 eV to 1 keV, auroral electrons [Gurnett and Frank, 1972]. These electrons are believed to be part of the primary field-aligned current circuit that couples the outer magnetosphere to the auroral ionosphere. As presently understood, the auroral hiss is generated by Cerenkov radiation from the suprathermal auroral electron beam, possibly amplified by coherent processes [Maggs, 1976]. Because auroral hiss is generally regarded as a reliable indicator of suprathermal electron beams in the Earth's auroral zones, the observation of auroral hiss at the edge of the Io plasma torus is strongly suggestive of intense electron beams in this region of the Jovian magnetosphere. Most likely these electron beams would be associated with a Birkeland (field-aligned) current linking the Io torus with the Jovian ionosphere as illustrated in Figure 8.18. Because the auroral hiss appears to be propagating toward the equatorial plane, the electron motion would have to be in the same direction, corresponding to a field-aligned current directed away from the equatorial plane. At the

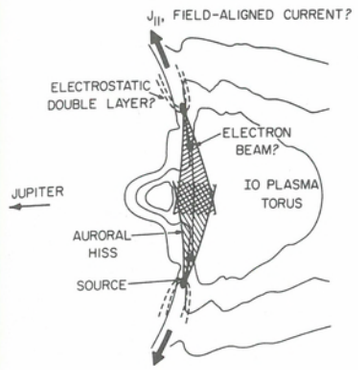

Fig. 8.18. A schematic illustration of the auroral hiss source region inferred from the low-frequency cutoff of the auroral hiss. Based on analogy with auroral hiss observed in the Earth's magnetosphere, this noise indicates the presence of an intense beam of low-energy (10 eV to 1 keV) electrons at the inner edge of the hot torus, possibly accelerated in a region of parallel electric fields (electrostatic double layer) near the edge of the torus.

present time, no evidence is available supporting the existence of such a current. However, the magnetic field is quite strong in this region, and the magnetic field perturbation caused by an electron beam of 10^8 to 10^{10} electrons cm^{-2} would be difficult to detect with the Voyager magnetometer (M. Acuña, personal communication).

If field-aligned currents are present at the inner edge of the Io torus, these currents would probably be caused by a divergence in the perpendicular current system at the torus boundary, with a resultant charge build up and acceleration of particles along the magnetic field lines. The acceleration process would be very similar to the terrestrial auroral electron acceleration, with the torus plasma playing a role similar to the terrestrial ionosphere. The abrupt termination of the auroral hiss source at a distance of about 0.65 R_J from the equator may in fact be directly indicative of the electron acceleration region. For terrestrial auroral hiss the sharp V-shaped low frequency cutoff has been widely interpreted as giving the location of the auroral electron acceleration region [Shawhan, 1979], possibly associated with the formation of an electrostatic double layer as illustrated in Figure 8.18.

8.6. Broadband electrostatic noise

During both the inbound and outbound passes of Voyager 1 and 2 several regions of intense low-frequency electric field noise were encountered near the outer boundary of the plasma sheet [Barbosa et al., 1981] with characteristics very similar to a type of noise observed in the Earth's magnetosphere called broadband electrostatic noise [Gurnett, Frank, and Lepping, 1976]. A representative example of this noise is shown in Figure 8.19. Typically, this noise has a broad frequency spectrum extending more or less monotonically from less than 10 Hz to greater than 1 kHz. A distinguishing characteristic of this noise is the spiky appearance in the wideband frequency-time spectrograms, with many impulsive vertical features, as in the bottom panel of Figure 8.19. It is this spiky appearance that leads us to believe that the noise is electrostatic; the comparable type of noise in the Earth's magnetosphere has a negligible magnetic component and is also spiky. Although the noise occurs in a frequency range where the whistler-mode can propagate, it is unlikely that the noise is propagating entirely in the whistler mode because the magnetic field is very small and the noise sometimes extends to frequencies well above the electron cyclotron frequency. Unfortunately, even in the Earth's magnetosphere we have little precise knowledge of the mode of propagation. The very broad frequency spectrum and spiky appearance suggest that the noise may consist of short wavelength waves that are strongly Doppler shifted.

In the Earth's magnetosphere the broadband electrostatic noise is known to be associated with boundaries that carry large field- aligned currents, such as the bound-

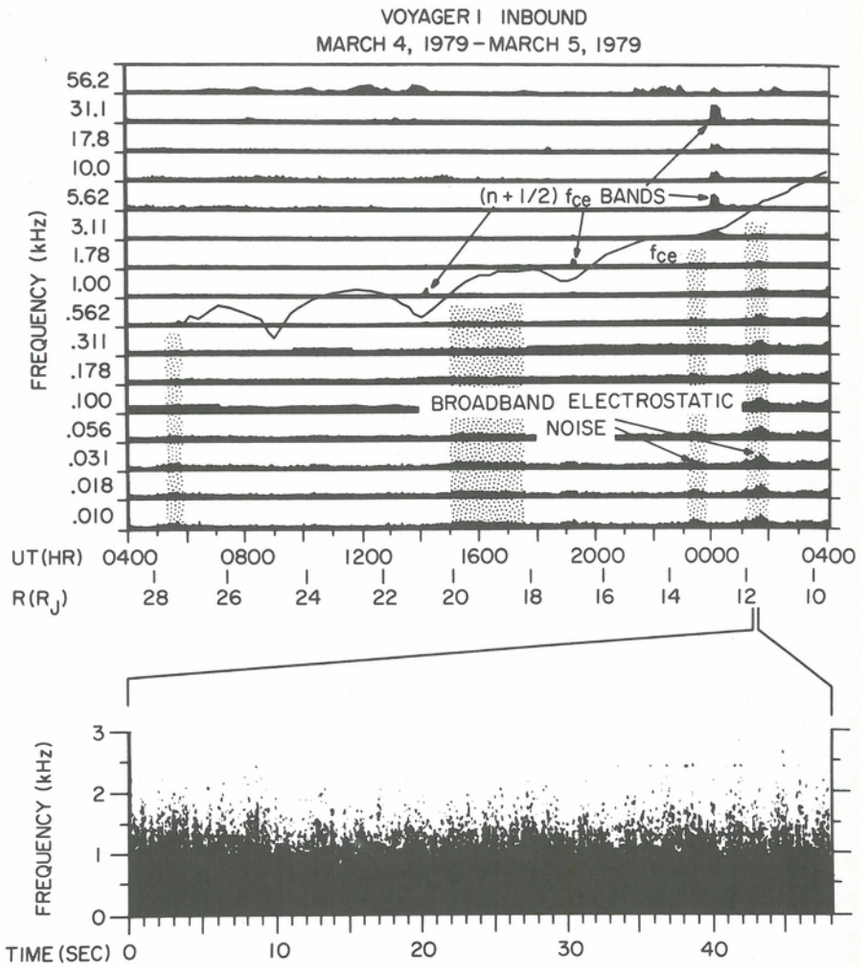

Fig. 8.19. An example of the broadband-electrostatic noise detected near the outer boundary of the plasma sheet. This noise has a broad frequency spectrum and is very spiky, indicating that the noise consists of short-wavelength electrostatic waves.

ary of the plasma sheet [Gurnett, Frank, and Lepping, 1976], the auroral field lines [Gurnett and Frank, 1977], the polar cusp [Gurnett and Frank, 1978b] and the magnetopause [Gurnett et al., 1979a]. At Jupiter, the broadband electric-field noise also appears to be associated with boundaries. Barbosa et al. [1981] demonstrate that broadband electrostatic noise occurs near the outer boundary of the Jovian plasma sheet. For example, the two regions of broadband electric field noise at 2320 and 0140 UT in Figure 8.19 are symmetrically located north and south of the magnetic equator (which can be identified from the $3 f_{ce}/2$ and UHR emissions). The broadband electrostatic noise events occur at peaks in the plasma density that have been interpreted as a bifurcation in the north–south density profile of the plasma sheet [McNutt, Belcher, and Bridge, 1981]. During the dayside crossing of the magnetopause by Voyager 2 a similar type of broadband noise was also identified near the magnetopause [Gurnett, Kurth, and Scarf, 1979a]. The overall morphology of the broadband electrostatic noise is,

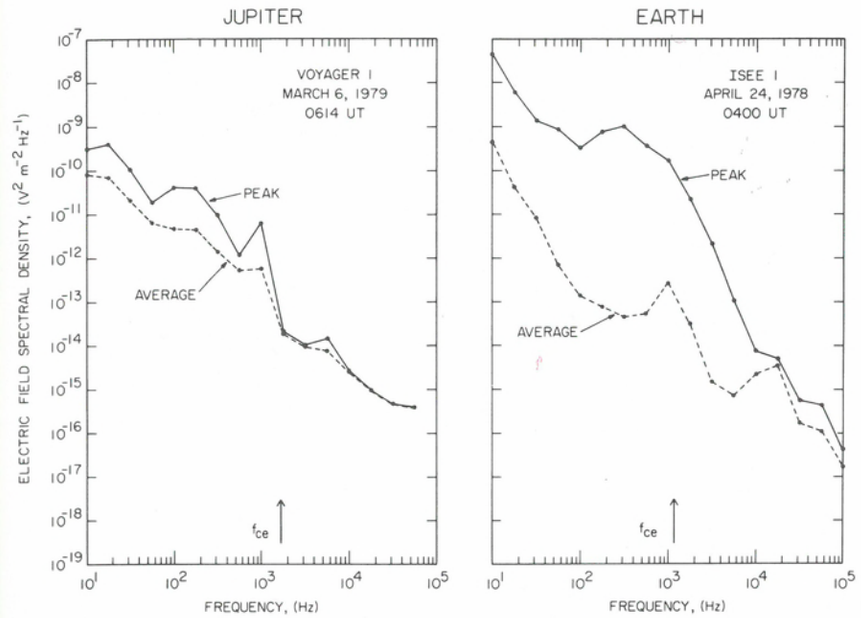

Fig. 8.20. A comparison of the spectra of broadband-electric-field noise observed near the boundary of the Jovian and terrestrial plasma sheets. The Jovian broadband-electrostatic noise generally occurs at lower frequencies and has lower intensities than the comparable noise in the terrestrial magnetosphere [from Barbosa et al., 1981].

therefore, quite similar at Earth and Jupiter, with a strong tendency for the noise to occur near boundaries that carry field-aligned currents.

A comparison of the frequency spectrum of the broadband electrostatic noise at Earth and Jupiter is shown in Figure 8.20. In both cases the spectra were obtained from the outer boundary of the plasma sheet on the evening side of the magnetosphere. As can be seen, the form of the frequency spectrum is very similar at both planets, with the intensity generally decreasing toward increasing frequency approximately as $f^{-2.0}$. In some cases, a distinct break occurs in the slope of the spectrum near the electron gyrofrequency. The electric-field intensities at Jupiter are usually significantly smaller than at Earth, as if the basic spectrum were shifted downward in frequency by about a factor of 10. A downward shift in the frequencies at Jupiter is probably not surprising as all of the characteristic frequencies of the plasma in the Jovian plasma sheet are substantially lower than in the terrestrial plasma sheet.

Among the various magnetospheric plasma wave processes that have been discussed, the broadband electrostatic noise is probably the least well understood. At present, only two mechanisms have been proposed to explain this noise. Ashour-Abdalla and Thorne [1977] have suggested that the noise may be caused by electrostatic ion-cyclotron waves driven by a loss-cone instability, and Huba, Gladd, and Papadopoulos [1978] have suggested that the noise may be caused by a lower-hybrid drift instability driven by the cross-field current. Both of these mechanisms would require large Doppler shifts to explain the observed frequency spectra. Because the noise seems to be associated with field-aligned currents, it also appears that current-driven instabilities, such as the current-driven ion-cyclotron instability [Kindel and Kennel, 1971] should be considered. Electrostatic ion-cyclotron waves have been identified in association with auroral field-aligned currents at relatively low altitudes in

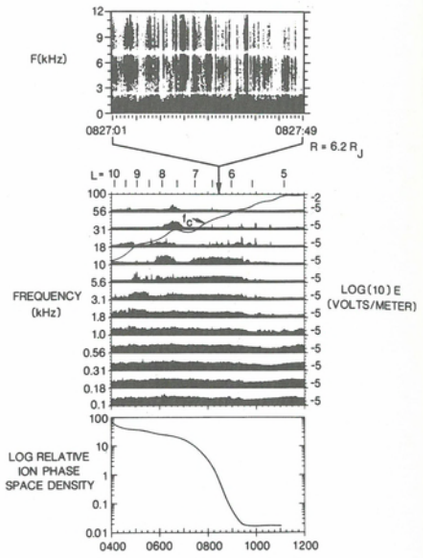

Fig. 8.21. Evidence of intense electrostatic waves in the Io plasma torus. The strong impulsive bursts extending from ~3 to 10 kHz in the top panel are believed to be short wavelength electrostatic waves. These waves occur in a region where the energetic ion phase-space density decreases rapidly, suggesting that these waves may cause precipitation of energetic ions.

the Earth's magnetosphere [Kintner, Kelley, and Mozer, 1978]. Whether waves of this type can account for the broadband electrostatic noise observed at much higher altitudes in the magnetosphere remains to be determined.

Probably the most important implication of the Jovian broadband electrostatic noise is that this noise provides indirect evidence of substantial field-aligned currents flowing along the boundary of the plasma sheet. In the Earth's magnetosphere a substantial body of evidence suggests that the broadband electrostatic noise is associated with field-aligned currents [Gurnett and Frank, 1977]. Although a full understanding of the plasma instability involved in the generation of this noise is not yet available, it can reasonably be presumed to be a current-driven instability. The observation of broadband electrostatic noise along the outer boundary of the Jovian plasma sheet is in close agreement with terrestrial observations, suggesting that a field-aligned current system links the Jovian plasma sheet to the auroral ionosphere in a manner similar to the auroral current system in the terrestrial magnetosphere.

8.7. Discussion

Although the general characteristics of the Jovian plasma wave phenomena can now be regarded as reasonably well understood, numerous detailed observational and theoretical questions remain. For example, although detailed particle loss rates have been computed, it is still not certain that the chorus and hiss emissions are entirely responsible for the particle precipitation and aurora observed at the foot of the torus field lines. Goertz [1980a] has pointed out that the energetic electron diffusion and energy transport rate into the torus is too small by about a factor of 10 to account for the energy precipitated in the aurora (see Chap. 12). Thus, it is questionable whether electron scattering by whistler-mode waves in the torus can account for the torus aurora. It appears more likely that proton precipitation by electromagnetic ion-cyclotron waves or some other type of wave-particle interaction could account for the observed auroral light intensities. Unfortunately, the Voyager plasma-wave instrument does not extend to sufficiently low frequencies to determine whether ion-cyclotron waves are present. In a possibly related development, Scarf, Gurnett, and Kurth [1981] have recently presented observations suggesting that significant levels of electrostatic noise may also exist in the torus, superimposed on the whistler-mode hiss. The top panel of Figure 8.21 shows one example of the impulsive spectral characteristics that are believed to be indicative of short wavelength electrostatic waves in the Io plasma torus. The broad bandwidth of the individual bursts could be caused by large Doppler shifts as the corotating plasma sweeps past the spacecraft. The central panel in Figure 8.21 shows part of the 16 channel survey data during the inbound passage through the Io torus. The uniformly enhanced wave levels detected in the 3.1 to 10 kHz channels before about 0927 UT are thought to be caused by these broadband electrostatic noise bursts.

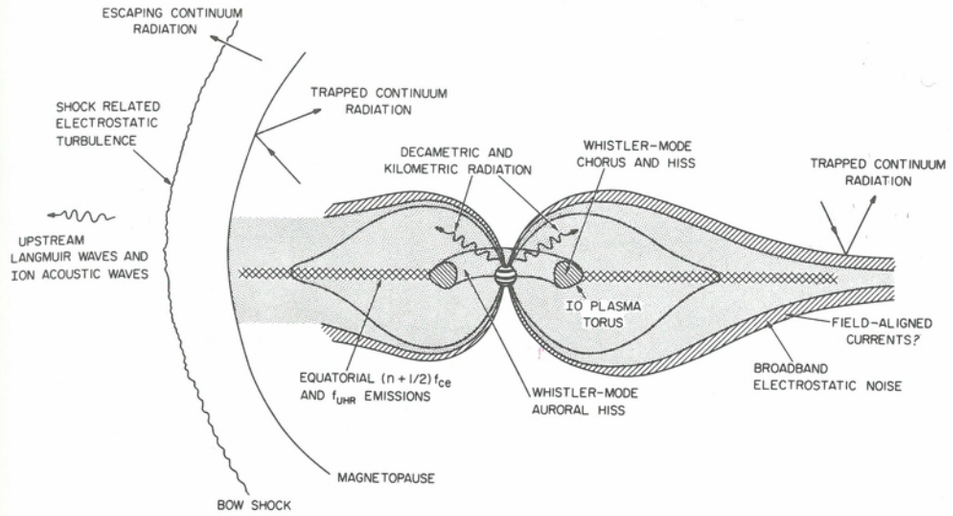

Fig. 8.22. A summary of the principal types of plasma waves detected by Voyager and their regions of occurrence.

The possible role that this electrostatic noise could play in the torus dynamics is not understood. However, the phase space density plot in the bottom panel in Figure 8.21 [adapted from Armstrong et al., 1981] shows that significant ion precipitation developed in the region where the electrostatic noise is present. Because the ion losses stopped just where the wave turbulence ended, it is quite possible that this electrostatic noise plays a role in precipitating energetic ions and thereby producing the aurora at the foot of the Io field lines.

Another unresolved issue involves the observation of auroral hiss at the inner edge of the Io torus. As discussed earlier, the presence of auroral hiss is thought to indicate the presence of field-aligned particle beams and currents in this region, possibly including the formation of electrostatic double layers along the field lines. Is it possible that these particle beams and currents contribute to the torus aurora? At the present time, essentially nothing is known about the suprathermal particles responsible for the auroral hiss, other than what can be concluded from the general similarity to terrestrial auroral hiss.

Substantial questions still remain concerning the continuum radiation observed in the Jovian magnetosphere. How is this radiation generated? Is the mode conversion discussed by Melrose [1981] adequate for explaining the continuum radiation, or is some other process necessary? What is the Q factor of the magnetospheric cavity for the trapped continuum radiation, and how much radiation escapes down the tail?

Table 8.2. *Jovian plasma waves*

Name	Region of occurrence	Frequency range	Representative broadband electric field strength	Plasma wave mode	Free energy source
Upstream ion-acoustic waves	Upstream of bow shock	$f \simeq (V_s/\lambda) \cos\theta$, 100 Hz to 3 kHz	10 to 30 μV m^{-1}	Ion-acoustic-like mode	Ion beams from bow shock
Upstream electron plasma oscillations	Upstream of bow shock	$f \simeq f_{pe}$, ~3 to 5 kHz	10 to 100 μV m^{-1} (very impulsive)	Langmuir mode	Electron beam from bow shock
Bow shock noise	Bow shock	Broadband 10 Hz to ~10 kHz	1 to 3 mV m^{-1}	Ion-acoustic or Buneman mode, whistler mode and Langmuir mode	Current in bow shock, beams and anisotropies generated in shock
Continuum radiation	Magnetospheric cavity	$f > f_{pe}$, 20 Hz to ~10 kHz	See Fig. 8.8	Free space (R,X) and (L,O) modes	Coupling from electrostatic UHR emissions
UHR emissions	Magnetic equator and Io torus	$(n + 1/2) f_{ce} \simeq f_{UHR}$, 1 to 400 kHz	3 to 10 mV m^{-1}	Z-mode, or electron Bernstein mode at UHR	$\partial f_e/\partial v_\perp > 0$, instability depends on n_c/n_H
Electron cyclotron waves					
(a) Discrete	Magnetic equator	$f \simeq 3/2\, f_{ce}$, $5/2\, f_{ce}$; 1 to 30 kHz	1 to 3 mV m^{-1}	Electron Bernstein mode	$\partial f_e/\partial v_\perp > 0$, instability depends on n_c/n_H
(b) Diffuse	Io plasma torus	$f = (n + 1/2) f_{ce}$ near f_{UHR}, 50 to 500 kHz		Electron Bernstein mode	Thermal excitation, or $\partial f_e/\partial v_\perp > 0$
Whistlers	Io plasma torus	$f \simeq f_{ce}$, 1 to 7 kHz	30 μV m^{-1}	Whistler mode	Lightning
Chorus	Io plasma torus	Near $f_{ce}/2$, ~8 to 12 kHz	0.3 mV m^{-1}	Whistler mode	Electron loss cone anisotropy, resonant energy few keV
Hiss	Io plasma torus	$f \lesssim f_{ce}$, 10 Hz to 10 kHz	1 to 2 mV m^{-1}	Whistler mode	Electron loss cone anisotropy, resonant energy few hundred keV
Auroral hiss	Io plasma torus	$f \lesssim f_{ce}$, 1 to 10 kHz	10 to 30 μV m^{-1}	Whistler mode	Electron beam, 10 eV to 10 keV
Broadband electrostatic noise	Outer boundary of plasma sheet	10 Hz to 1 kHz	See Figure 8.20	Unknown, possibly ion cyclotron or LHR drift mode	Unknown, probably field-aligned currents

Could the tail be sufficiently long to allow the "trapped" continuum radiation to escape freely out the tail in regions of low solar wind plasma density downstream of Jupiter?

Because of limitations of the Voyager instrumentation, the electron distribution functions responsible for the $(n + 1/2)\, f_{ce}$ and f_{UHR} waves have not yet been determined. A basic question, therefore, remains as to why these waves are so closely confined to the magnetic equator. Is the equatorial confinement indicative of a highly anisotropic angular distribution that occurs only at the magnetic equator, or is the equatorial confinement a propagation effect? Can equatorial upper hybrid emissions account for the narrowband kilometric radiation by processes similar to the generation of the continuum radiation? Similarly, in the plasma sheet basic questions remain concerning the broadband electrostatic noise. How is this noise generated? Is the noise indicative of field-aligned currents linking the plasma sheet to the auroral ionosphere? If so, what role does this turbulence play in high latitude auroral processes? Does the noise produce sufficient anamolous resistivity to cause field-aligned potential drops, ion-acceleration, and plasma heating effects similar to the processes believed to be occurring in the terrestrial magnetosphere?

In conclusion, it is clear that the Voyager observations have added greatly to our knowledge of plasma wave and radio emission processes in the Jovian magnetosphere. Table 8.2 and Figure 8.22 summarize the many types of waves observed and their regions of occurrence. Although in most cases a first-order understanding is available to account for the generation of these waves, questions still remain concerning the possible role that these waves play in the physics of the Jovian magnetosphere.

ACKNOWLEDGMENTS

We would like to extend our thanks to W. Kurth, R. R. Anderson, and R. West for their assistance in preparing illustrations of the Voyager and ISEE data and for their helpful discussions concerning the interpretation of the data.

The research at The University of Iowa was supported by NASA through Contract 954013 with the Jet Propulsion Laboratory and through Grants NGL-16-001-002 and NGL-16-001-043 with NASA Headquarters and by the Office of Naval Research. The research at TRW was supported by NASA through Contract 954012 with the Jet Propulsion Laboratory.

9

THEORIES OF RADIO EMISSIONS AND PLASMA WAVES

Melvyn L. Goldstein and C. K. Goertz

A generally accepted theory of the enigmatic phenomenon of planetary radio emission is not yet available. In this chapter, we direct our attention primarily to the question of how the Jovian decameter radiation might be generated via both direct and indirect mechanisms. Direct mechanisms transform the free energy contained in an electron distribution (typically a loss-cone) directly into electromagnetic waves. Indirect mechanisms transform the free energy contained in an electron beam distribution first into electrostatic waves that can then couple, in some manner, to produce electromagnetic waves. The growth rates for the unstable electromagnetic and electrostatic waves are derived. Nonlinear theories are briefly discussed as they apply to the case of Jupiter's decametric radiation. Because most of the Jovian radio emission seems to be controlled by Io, we describe how Io, through the emission of kinetic Alfvén waves, can produce a "beamlike" electron distribution. It is more difficult to understand how Io can enhance or produce a "loss-cone" distribution. Thus we conclude that, at least for Jovian radio phenomena, indirect mechanisms are preferred. We also describe theories and models for the generation of the dynamic spectral arcs that characterize the radio spectrum from hectometric to decametric wavelengths.

9.1. Introduction

Jupiter is the most powerful planetary source of nonthermal electromagnetic radiation in the solar system, with a radio spectrum extending from a few kHz to over 100 MHz. The phenomenology of the decimeter component in the GHz range has been discussed in Chapter 7. Here we concentrate on the complex region of Jupiter's spectrum at decameter wavelengths, the so-called DAM. The relevant observations are described in Chapters 7 and 8 and we reference them freely.

Theoretical interpretations of Jupiter's low frequency radio emissions have been plentiful and imaginative, ranging from the suggestion by Vasil'ev, Volovik, and Zalyubovskii [1972] that extensive air showers of ultrarelativistic cosmic rays impinging on the Jovian atmosphere coherently excite the observed radio frequencies, to more prosaic proposals relating the observations to plasma instabilities well known from laboratory and space physics. However, owing perhaps to the rich and detailed phenomenology and fascinating morphology, or perhaps to our limited but rapidly increasing knowledge of the physical environment of Jupiter's magnetosphere and upper ionosphere, there are as yet no theories of any of the low frequency radio components that are generally accepted as being completely correct. This is in contrast to the situation at decimeter wavelengths, where, as pointed out in Chapter 7, a rather coherent picture of the emission mechanism has been formulated. As we shall see, however, some aspects of the observations at decameter wavelengths do appear consistent with at least some of the theories.

There is something of a renaissance of interest in this area of research as the results of the Voyager missions are digested and assimilated. In the following discussion, we emphasize the basic theoretical ideas that underly both the older and newer theories and models, and thus provide a suitable foundation for understanding the latest literature. In this chapter, we follow Smith [1976a] in using the term "phenomenology" to